Innate Immunity and the Retinal Pigment Epithelium in Gene Therapy for Inherited Retinal Disorders

by

Geoffrey Alexander Casey

A thesis submitted in partial fulfillment of the requirements for the degree of

Master of Science

Medical Sciences - Medical Genetics
University of Alberta

ABSTRACT

Background: The photoreceptors are post-mitotic (no longer dividing), so the eye has evolved several unique immunological mechanisms to protect the photoreceptors and prevent vision loss. Inherited retinal disorders occur when mutations disrupt normal retinal function and photoreceptors die. Choroideremia is an inherited retinal disorder that is currently incurable, although several therapies are in development. Choroideremia and other inherited retinal disorders are candidates for viral gene therapy, where engineered viruses deliver therapeutic "wild-type" (normal) copies of mutated genes to target cells, restoring normal function. Many such therapies are now in clinical trials, but the results of some early trials suggest that the immune response of the retina against viral gene therapy vectors is not well understood and is likely limiting efficacy and decreasing the safety of the treatment.

Purpose: This study was designed to evaluate the innate immune response of the retinal pigment epithelium (RPE) against adeno-associated virus (AAV) and equine infectious anemia virus (EIAV) vectors, two vector platforms commonly used in ocular gene therapy. I hypothesize that AAV and EIAV vectors will stimulate an innate immune response in human RPE when detected by Toll-like receptor 9 and Toll-like receptor 3, respectively.

Methods: RPE derived from induced pluripotent stem cells (iPSC-RPE) was grown in culture until it demonstrated markers of functional, mature RPE, including pigmentation, polarization, polygonal morphology, and fluid pumping capability. Cells were treated with analogues of viral RNA and DNA (Poly(I:C) and CpG-DNA, respectively), the anti-viral cytokine IFNγ, or viral vectors. Levels of secreted immune response proteins (IL6, IL8, or CCL2) were measured via enzyme-linked immunosorbent assay (ELISA) analysis of harvested cell culture media. At the terminal time point for each sample, RNA was extracted and purified

before RT-qPCR expression level analysis of several pro-inflammatory and anti-viral genes (*IL6, IL8, CXCL10, RSAD2*, and others).

Results: While Poly(I:C) and IFNγ stimulated upregulation of several pro-inflammatory and anti-viral genes and increased secretion of IL6, IL8, and CCL2 to varying degrees, treatment with viral vectors resulted in very low transduction efficiency (GFP transgene expression observed in an estimated <1% of all cells). As a result, most changes in gene expression failed to reach statistical significance.

Conclusions: To increase the predictive capability of this study, it must be repeated with a higher ratio of viral particles to target cells (multiplicity of infection or "MOI") before conclusions can be drawn. While many trends in the data agree with previously published findings from other cell types *in vitro* and model organisms *in vivo*, the low transduction efficiency prevents deeper analysis.

DEDICATION AND ACKNOWLEDGEMENTS

I would like to thank my committee members, Dr. David Evans and Dr. Michael Walter, for all their advice and guidance on this project. Your enthusiasm has been contagious, and I appreciate the time and effort that you have given me. You were part of the reason that my time in the Department of Medical Genetics was such a positive experience, and I truly thank you for that.

I would like to sincerely thank my supervisor, Dr. Ian MacDonald, for his guidance, patience, and help during my time in his lab. Dr. MacDonald allowed me to follow my curiosity on this project, even when it felt like our hypotheses challenged the "status quo" in gene therapy. More than that, Dr. MacDonald has been incredibly generous and kind, facilitating all kinds of opportunities for learning, even during tough times. Dr. MacDonald, I can never thank you enough for everything you have done for me over the past 5 years. Thank you.

Finally, I would like to thank my incredible support system of lab members, friends, and family for supporting me through this project. This project has had its fair share of high points and low points but having you by my side to enjoy the good times and weather the bad times has made all the difference to me. To my siblings, Sean and Alison, thank you for all your support. You both mean the world to me and have helped me in ways you cannot even imagine. To my partner Stephanie and our dog Olive, thank you for celebrating with me or crying with me whenever I needed, and for taking care of me when I got busy and forgot to take care of myself. To my mom, Linda, I can never thank you enough. I would not have made it 3 months into this journey without you acting as my therapist, editor, financier, and cheerleader; knowing that you are always in my corner made this possible. I love you all so much; this work is dedicated to all of you and to my dad, Ron.

TABLE OF CONTENTS

LIST OF TABLES

LIST OF FIGURES

LIST OF ABBREVIATIONS/SYMBOLS

°C	degrees Celsius
AAV	adeno-associated virus
AMD	age-related macular degeneration
aPES	asymmetric polyethersulfone
BBB	blood-brain barrier
BRB	blood-retina barrier
CHM	choroideremia (gene)
CHM	Choroideremia (disorder)
CHML	choroideremia-like (gene)
CNS	central nervous system
DME	diabetic macular edema
DNA	deoxyribonucleic acid
dsDNA	double-stranded DNA
dsRNA	double-stranded RNA
EIAV	equine infectious anemia virus
FBS	fetal bovine serum
g	gram
GFP	green fluorescent protein
HPLC	high performance liquid chromatography
hpt	hours post-transduction
HCQ	hydroxychloroquine
IF	immunofluorescence
IFBS	immunofluorescence blocking solution
ILM	inner limiting membrane
iPSC	induced pluripotent stem cell
iPSC-RPE	retinal pigment epithelium derived from induced pluripotent stem cells
kDa	kilodalton (equal to 1000 g/mol)
LCA	Leber congenital amaurosis
MEM α	minimum essential medium α (ThermoFisher Cat. No. 12571063)
nAMD	neovascular age-related macular degeneration
NHP	non-human primate
ONL	outer nuclear layer

PBS	phosphate buffered saline
PBST	phosphate buffered saline + 0.1% Tween 20
PEI	polyethylenimine
PET	polyethylene terephthalate
PFA	paraformaldehyde
PS	phosphatidylserine
rAAV	recombinant AAV (vector)
RCF	relative centrifugal force
REP-1	Rab escort protein-1 (protein)
REP-2	Rab escort protein-2 (protein)
RNA	ribonucleic acid
RP	retinitis pigmentosa
RPE	retinal pigment epithelium
RPM	rotations per minute
SAE	serious adverse event
SD-OCT	spectral domain optical coherence tomography
ssDNA	single-stranded DNA
ssRNA	single-stranded RNA
T_3	triiodo-L-thryonine
XLRS	X-linked retinoschisis

NOTE REGARDING THE NOVEL CORONAVIRUS PANDEMIC OF 2019-2021

In late 2019 and early 2020, the novel coronavirus SARS-CoV-2 caused a pandemic that slowed or stopped many industries worldwide, including scientific supply companies. As the demand spiked for PCR reagents, testing kits, and other common lab supplies, it became difficult or impossible to acquire these products for purposes other than COVID-19 testing. As a result, some of the experiments performed for the completion of this thesis faced unexpected hurdles, primarily from shortages of consumables such as Transwells, pipette tips, and media/supplements.

1. INTRODUCTION

1.1. The retina and choroideremia

The eye is a remarkably complex organ comprised of many different cell types. At the back of the eyeball is the retina, including the light-sensing photoreceptors and many types of support cells. The retina is a part of the central nervous system (CNS) and contains highly specialized post-mitotic cells including photoreceptors, bipolar cells, and others [1], [2]. There are ten layers in the retina; anterior-to-posterior, these layers are the inner limiting membrane (ILM), the nerve fiber layer, the ganglion cell layer (GCL), the inner plexiform layer (IPL), the inner nuclear layer (INL), the outer plexiform layer (OPL), the outer nuclear layer (ONL), the external limiting membrane, the photoreceptor layer, and the retinal pigment epithelium (RPE) [3]. There are three types of glial cells in the human retina; Müller glia, astrocytes, and microglia [4]. Müller glia and astrocytes are thought to primarily contribute to maintenance of homeostasis in the retina, with Müller glia providing structural support for other cell types and astrocytes monitoring and controlling retinal pH, among other functions. Microglia play a more defensive role, responding to sites of infection or damage and clearing toxic entities. Because of this role, microglia are typically protective, but because of their ability to rapidly secrete cytokines and phagocytose cells (including photoreceptors and other retinal cells), proper modulation of their activation is crucial for retinal health [4].

Choroideremia (CHM; OMIM #303100) is an X-linked ocular disorder caused by mutations in the *CHM* gene (*Xq21.2*) [5]. Choroideremia affects the outer retina, causing degeneration of the retina, RPE, and choroid. Patients experience night blindness followed by loss of peripheral vision and eventual blindness [5]. Choroideremia is considered an excellent candidate disease for gene therapy [6]. It is a monogenic disorder, which means that it is caused

exclusively by mutations in one gene (*CHM*); this allows for the "gene replacement" strategy of gene therapy, where all CHM patients receive the same therapeutic vector that introduces a wild-type copy of the mutated gene into patient cells. While CHM patients are missing functional copies of the *CHM* gene in all cells of their body, the disease exclusively manifests itself in the retina, with other tissues spared from the disease phenotype (a hypothesized reason for this tissue specificity is discussed below) [7]. As a result, only the affected cells in the retina need to be corrected by the gene therapy to "cure" the patient. The cornea is optically clear, which allows surgeons to precisely administer vector to the retina. Finally, each eye in treated model organisms (for pre-clinical work) or humans (for clinical trials) can be treated independently, and comparison of the disease progression in the treated eye against the untreated eye allows for measurement of the impact of the vector without concern of confounding variables between subjects (feeding, light exposure, genetic background, etc.). This study did not directly evaluate a CHM gene therapy vector nor the therapeutic implications of such a vector. It was initiated in response to a Phase I/II clinical trial of an AAV2.REP1 vector which reported minimal benefit to patients in terms of preventing disease progression and a serious adverse event (SAE) that one patient experienced after treatment. The SAE suggested that the innate immune response of the retina to viral gene therapy vectors is understudied, and this project was designed to attempt to fill that knowledge gap in the literature.

Chorideremia is caused by under-prenylation of small Rab GTPase ("Rab proteins" or "Rabs") proteins. Rabs are functional and contribute to intracellular vesicular trafficking when they are anchored to membranes within the cell, but they localize to the cytosol after translation. The re-localization to cellular membranes is facilitated by the addition of a hydrophobic geranylgeranyl group through a process called prenylation. The *CHM* gene codes for Rab escort

protein-1 (REP-1). REP-1 escorts the unprenylated Rabs to Rab geranylgeranyltransferase (RabGGTase) and escorts the Rabs to the target membrane after they have been prenylated. A homologue of *CHM* (*CHML*, for choroideremia-like) encodes Rab escort protein-2 (REP-2). REP-2 can also facilitate Rab prenylation; it has been hypothesized that functional REP-2 can compensate for the loss of REP-1 in all tissues except for the retina, potentially explaining the retina-specific phenotype in choroideremia patients [8].

The precise etiology of the disease is undetermined, but it is hypothesized to be due to under-prenylation of proteins and accumulation of damage in the retinal pigment epithelium and photoreceptors, two tissues known to be affected [9].

1.2. Retinal immune mechanisms and ocular immune privilege

Humans cannot regenerate photoreceptors that have been lost due to disease or trauma, and the human retina has unique immunological features to protect against photoreceptor loss. The retina is isolated from the vascular system by the blood-retina barrier (BRB), including the ILM and the RPE [10], [11]. The BRB allows immune protection in the retina via resident microglia and innate immune responses while carefully controlling inflammation, preventing irreversible damage to the post-mitotic photoreceptors [12].

The RPE is the outermost layer of the retina, and is a monolayer of cells connected by tight junctions [13]. As a result, the RPE acts as a "gatekeeper"; large molecules cannot diffuse between the cells of the RPE and passage into the retina can be selectively permitted or prevented [10]. Loss of functional RPE tight junctions (or loss of RPE cells entirely) results in increased permeability, permitting infiltration of leukocytes [10], [14].

The microglia reside in the inner and outer plexiform layers of the retina under normal resting conditions [15], [16]. When the retina is exposed to immune insult or is diseased,

however, the microglia are mobilized and translocate to the outer nuclear layer and subretinal space [16], [17]. The impact of activated microglia on the retina is complex, and microglia have been shown to be both protective and damaging to photoreceptors under different circumstances [17]–[20]. Other types of immune cells are normally absent from the retina [16]. Under abnormal conditions (disease, trauma, or immune insult), immune cell homeostasis in the retina is disrupted. Retinal detachment (separation of the photoreceptors and RPE) has been shown to trigger microglial migration to the outer nuclear layer and subretinal space in various species [21] and infiltration of bone marrow-derived (non-resident) macrophages [22] into the retina. The macrophages phagocytose apoptotic photoreceptors, removing debris from the retina. Phagocytosis of apoptotic photoreceptors by infiltrating macrophages or resident microglia is termed "secondary phagocytosis". In secondary phagocytosis, the neurons are irreversibly fated for programmed cell death due to insult [23]. Alternatively, phagocytosis of "stressed-but-viable" photoreceptors is termed "primary phagocytosis"; as their name suggests, stressed-but-viable neurons are under some type of stress but have not activated apoptosis. Both primary and secondary phagocytosis are stimulated by presentation of "eat-me signals" by the photoreceptors, including phosphatidylserine (PS), calreticulin, and others. In a retinitis pigmentosa (RP) mouse model, stressed photoreceptors demonstrate increased presentation of PS in the ONL, followed by infiltration of microglia [18], [24]. Without microglial migration to the ONL, survival rates of the stressed-but-viable photoreceptors (and retention of retinal function) improves, illustrating the importance of preventing microglial translocation [24].

The retinal pigment epithelium constitutively expresses Toll-like receptors (TLRs) 1-7, 9, and 10 [25], which allow the RPE to detect a range of pathogen-associated molecular patterns (PAMPs) or damage-associated molecular patterns (DAMPs). PAMPs are present on foreign

pathogens like bacteria, viruses, and fungi; DAMPs are molecules that indicate distressed/damaged cells of the same organism [26]. The TLRs enable the RPE to quickly mount an anti-bacterial, anti-viral, or anti-fungal response to minimize damage to the post-mitotic photoreceptors. TLRs 1, 2, 4, 5, 6, and 10 localize to the cell surface, while TLRs 3, 7, and 9 are intracellular, localizing to endosomes. Of particular interest for viral gene therapies are TLR3 and TLR9; TLR3 recognizes viral double-stranded RNA (dsRNA), while TLR9 recognizes unmethylated CpG motifs in bacterial and viral DNA. AAV-based viral gene therapy vectors are produced in bacteria and contain unmethylated CpG motifs, presenting a possible mechanism for patient cells to mount an immune response.

1.3. Gene therapy vectors

1.3.1. Recombinant adeno-associated virus vectors

To date, most viral vectors considered for ocular gene therapy applications have been based on adeno-associated virus and are called recombinant AAV (rAAV) vectors. rAAV vectors are composed of a single-stranded DNA (ssDNA) genome surrounded by an icosahedral protein capsid [27], [28]. Wild-type AAV is thought to be non-pathogenic in humans [29], but it is estimated that around 70% of the human population has been exposed to AAV and have developed neutralizing antibodies against the virus [28]. The AAV genome can incorporate a transgene of approximately 4.7 kb [30]. After transduction, the AAV genome remains episomal (does not integrate into the host genome) [31]. Recombinant AAV vectors are replication-deficient, which means that the genome that is incorporated into the final AAV particle lacks the helper and packaging genes required to produce new viral particles in transduced cells, an important feature for gene therapy vectors [28]. Reports of immune responses against AAV

vectors have been inconsistent, but some studies have indicated potential transgene silencing and/or immune responses against these vectors when delivered at therapeutic doses [32].

1.3.2. Equine infectious anemia virus vectors

Equine infectious anemia virus (EIAV)-based vectors are lentiviral retrovirus RNA vectors, composed of two single-stranded RNA (ssRNA) genomes complexed with reverse transcriptase (RT) protein and integrase (IN) protein. Unlike AAV vectors, the viral genome of EIAV vectors integrates into the host genome, creating the possibility of insertional mutagenesis [6]. The genomes, RT, and IN are enveloped in plasma membrane. EIAV-based vectors (and lentiviral vectors in general) are not as widely used as AAV-based vectors, but several have made it to clinical trial, including StarGen for the treatment of Stargardt disease [33] and RetinoStat® for the treatment of neovascular age-related macular degeneration [34]. While not an EIAV-based system, other retroviral vectors have been successful in clinical trials, including one dramatic case involving a patient with junctional epidermolysis bullosa, which is caused by mutations in genes important for skin lamination [35]. Keratinocytes from this patient were genetically corrected by retroviral vectors carrying wild-type *LAMB3*; because retroviruses integrate into the host genome, skin grafts with the genetic correction could be grown *ex vivo* and re-grafted onto the patient, with all daughter cells carrying the corrective transgene. At the time of admission to the hospital, the patient had lost over 60% of his epidermis; after re-grafting of the corrected epidermis, the patient regenerated approximately 80% of his skin surface area and the epidermis showed dramatically improved adhesion [35]. This clearly demonstrates the utility of integrating vectors for gene therapy applications in dividing cells but comes with the caveat that extensive lineage tracing and insertion analysis had to be performed to ensure that the patient did not receive grafted cells that were or could become cancerous.

1.3.3. Routes of administration and implications for therapy

Ocular gene therapy vectors are typically administered to the patient via subretinal injection or intravitreal injection [6]. In subretinal injections, a "bleb" of vector and carrier fluid is injected into the subretinal space between the outer nuclear layer of the photoreceptors and the RPE. Physical contact of the photoreceptors and RPE is restored as the RPE reabsorbs the carrier fluid. Subretinal injections permit efficient transduction of the outer cell layers (including the photoreceptors and RPE), as the vector physically bypasses the BRB and reaches target cells directly [36]. The injection procedure, however, compromises the BRB at the point of injection, and even transient retinal detachments lead to inflammation and photoreceptor loss [37]–[39]. In intravitreal injections, conversely, the vector is injected into the vitreous humor (the jelly-like fluid that fills the interior of the eyeball) and diffuses into the retina [6]. This route of administration is significantly less invasive, as the BRB is not compromised and the retina maintains constant contact with the underlying RPE. Intravitreally-injected vectors, however, must diffuse across the ILM and through inner layers of the retina to reach the outer retina/RPE. Most conventional AAV vectors do not penetrate deeply into the retina, limiting their applicability for some ocular disorders [36]. Additionally, intravitreally-injected vectors are introduced outside of the BRB; non-human primate studies have shown that intravitreal injections (but not subretinal injections) of vector stimulate can stimulate adaptive immune responses [40], [41].

1.3.4. Adverse events and inflammation

The Alberta Ocular Gene Therapy Team at the University of Alberta performed subretinal injections of rAAV2.REP1 (1×10^{11} vector genomes) in the worse eye of six CHM patients (ClinicalTrials.gov NCT0207736) [42]. Of these patients, none gained appreciable

visual function as of their two-year follow-up testing. One patient experienced intraretinal inflammation, which presented as hyperreflective spots in and around the macula on spectral domain optical coherence tomography (SD-OCT) follow-up one-month post-injection. The inflammation was controlled with oral prednisone, but the incident caused permanent damage. Other clinical trials for AAV-based gene therapies administered by subretinal injection also reported adverse events involving inflammation. A trial by the University of Oxford (ClinicalTrials.gov NCT01461213) reported severe adverse events in 2 out of 14 patients, of which one patient experienced significant inflammation that was "most likely vector-related" [43]. These patients had to be removed from the trial for intervention. A clinical trial at University College London (ClinicalTrials.gov NCT00643747) of the rAAV2/2.hRPE65p.hRPE65 vector for the treatment of Leber's Congenital Amaurosis (LCA) injected 1 x 10^{11} vector genomes ("low dose", n = 4) or 1 x 10^{12} vector genomes ("high dose", n = 8) into the subretinal space of 12 patients [44]. While no inflammation was detected in the low dose cohort, 5 of the 8 patients in the high dose cohort demonstrated some degree of inflammation; the impact on 4 of these patients was deemed nondeleterious, while one patient suffered irreversible loss of vision. Interestingly, this patient demonstrated an increase in anti-AAV2 immunoreactivity (neutralizing antibodies and T cells against AAV2). Similar increases in neutralizing antibodies were observed in studies with intravitreal AAV injections in NHPs, but not intraretinal injections; this suggests that shedding of the vector because of permeabilization of the BRB or leakage during the injection procedure is immunogenic.

Recently, ClinicalTrials.gov trial NCT04418427 reported a "Suspected Unexpected Serious Adverse Reaction" in a patient who received a high dose (6 x 10^{11} vector genomes) of AAV.7m8-aflibercept for the treatment of diabetic macular edema. The trial was unmasked after

the patient developed “hypotony, with panuveitis and loss of vision in the treated eye” 30 weeks post-treatment (https://finance.yahoo.com/news/adverum-biotechnologies-provides-infinity-trial-200100621.html, accessed May 22, 2021).

To-date, innate immunity in the retina has been relatively understudied for many reasons. Innate immune responses have not hindered pre-clinical testing of AAV-based ocular gene therapy vectors to a significant degree, and in some cases, animals demonstrating immune responses to these vectors are simply removed from their respective studies. The dogma of ocular immune privilege and the lack of a clinically relevant immune response to wild-type AAV in humans suggested that the immune response, if any, would be manageable and non-deleterious. The adverse events reported by gene therapy clinical trials, however, indicate that the immunogenicity of ocular gene therapy vectors merits thorough investigation and characterization. Efficacy of viral vectors and the magnitude of the immune response against them are inherently linked; efficacy/transduction efficiency can be increased by administering increasing quantities of vector to target tissues, but this increase in the desired outcome will be accompanied by an increase in innate immune reaction. The viral vectors share capsid/envelope proteins, genomic structure, and modes of cell infiltration with wild-type viruses, so an innate immune response should be expected.

Safe and effective gene therapy will require an intimate understanding of the mechanisms by which retinal cells recognize and respond to these markers of viral infection. As discussed, immunity in the retina is unique because of the post-mitotic nature of photoreceptors; the retina cannot mount a massive inflammatory response to viruses present within the BRB because the risk of permanent loss of photoreceptors is too great. Systemic or local immunosuppression with

steroids or other drugs is an option, but they have thus far failed to provide a guarantee of safety to patients.

1.4. Experimental Design and Treatment Rationale

This project attempted to characterize the response of the retinal pigment epithelium against gene therapy vector treatment and to propose adjustments in vector design, delivery, or adjuvant treatments that will improve the safety profile of future ocular gene therapy clinical trials. The experimental designs below were designed to build upon the findings of Zhao et al. [18], Brosig et al. [45] and Chandler et al. [46]. The insights provided by each study and their contributions to the design of this study are detailed below.

Aim 1: Study changes in gene expression regulation in retinal pigment epithelial cells derived from induced pluripotent stem cells after treatment with viral RNA and DNA analogues.

Brosig et al. studied the innate immune response of primary human RPE. Human primary RPE cells were in culture for 4-5 days before treatment with polyinosinic:polycytidylic acid (Poly(I:C), an agonist of Toll-like receptor 3) or CpG-DNA (a synthetic oligonucleotide agonist of TLR9). The authors reported that these primary RPE responded to Poly(I:C) stimulation (100 – 500 µg/mL) with a dose-dependent upregulation of proinflammatory genes, including *TLR2, TLR3, RELA, IL6,* and *CCL2* (among many others). They detected *TLR9* expression via RT-qPCR but did not detect any significant changes in gene expression after treatment with 500 nM CpG-DNA. These data were relevant to ocular gene therapy because several gene therapy vectors (including the EIAV.GFP vector used in this study) have RNA genomes. These findings suggest that the RPE can detect a viral RNA genome via TLR3 and mount an anti-inflammatory response.

To expand on the Brosig report, the experimental design was modified in two major ways. First, the Brosig study used "near-confluent" or "confluent" cultures of primary human RPE from twelve females and twenty-nine males who were nineteen to eighty-five years old. The authors reported no significant differences when adjusting for sex or age of the donor. The RPE, however, did not reach homeostasis in culture before treatments were applied. As seen by the iPSC-RPE in culture (Section 3.1. RPE take time to acclimate to cell culture conditions and do not rapidly mature. All the samples in the Brosig study were isolated from donors within 48 hours post-mortem but were in culture for only 4-5 days. All primary cells have inherent variability and a study by Mazzonni, Safa, and Finnemann probed the utility of primary RPE in culture; they cautioned against drawing conclusions from cells cultured in this manner, stating that "[primary human RPE] generally require careful control of culture conditions to achieve re-polarization in culture, which occurs only over a relatively long period (often several weeks). The complexity of cell culture protocols may be the reason that few studies have been published exploring human RPE cells for mechanistic studies of the phagocytic pathway." [47]. To expand upon the Brosig et al. findings, this study utilized RPE grown in long-term culture to avoid any effects of the tissue handling immediately prior to treatment. While an alternative human RPE cell line called ARPE-19 is available from cell repositories, this cell line is spontaneously immortalized and requires long-term culture with specific conditions to achieve a mature RPE phenotype [48], and was therefore not utilized. Unlike primary RPE or ARPE-19 cells, however, the RPE used in this study were derived from induced pluripotent stem cells (iPSC-RPE), which were grown in culture for more than two months before treatment. Briefly, patient cells (fibroblasts) were reprogrammed to iPSC by nucleofection with plasmids that encode the Yamanaka factors (*MYC, OCT4, SOX2,* and *KLF4*, required for conversion to the iPSC state),

along with additional sequences to increase conversion efficiency [49]. These plasmids are available in as Addgene plasmids pEP4 EO2S EN2K (#20925), pEP4 EO2S ET2K (#20927), and pCEP4-M2L (#20926), and were nucleofected at a ratio of 3:3:2 per the protocol of Reichman et al. [49]. Once the fibroblasts were converted to iPSC, they were differentiated into RPE by replacing the iPSC-enforcing media with complete RPE media (Table 6). Approximately 8 weeks after converting to complete RPE media, pigmented foci began to appear, indicating differentiation to iPSC-RPE. These foci were manually isolated by dissection, separated into a single-cell suspension with trypsin and a cell strainer, and re-plated. The re-plated cells divided and formed pure cultures of iPSC-RPE, which were kept in culture for approximately 3 weeks before being frozen down and stored as stocks. The de-differentiation and reprogramming of these cells were completed in the lab of Dr. Viki Kalatzis (Montpellier, FRA), and the cells were received in our lab as the frozen, re-differentiated stocks. Long-term iPSC-RPE cultures offer many advantages over primary human RPE. First, primary human RPE undergoes significant stress as it is isolated from the donor and transitioned into culture. Many of the manipulations that the RPE experiences have the potential to cause dramatic changes in gene expression, including tissue excision, changes in temperature, and the adjustment to a new environment and food source. Additionally, the use of iPSC-RPE in culture meant that all samples came from a common donor and have the same genotype, age, and cell culture conditions. Long-term cultures of iPSC-RPE improve upon primary human RPE because they are allowed to stabilize and mature. I hypothesize that this will more accurately represent the response of native RPE without the confounding response introduced by the manipulation of primary RPE excision and plating. The second major modification that was made to the Brosig experimental design was the incorporation of viral vectors instead of only viral and bacterial RNA and DNA analogues. These

analogues can be very useful, but the use of viral vectors in this study hypothetically permitted evaluation of the correlation between innate immune response and the vector dosage required to achieve therapeutic levels of transduction.

Aim 2: Evaluate the time course of the pro-inflammatory/anti-viral response by iPSC-RPE to viral vectors *in vitro* and assess the impact of hydroxychloroquine on iPSC-RPE transduction and inflammatory response.

In a 2019 study by Chandler et al. [46], the time course of the *in vivo* innate immune response of the murine retina against AAV vectors was reported, with some surprising results. As detected by RT-qPCR, many different pro-inflammatory and anti-viral genes were expressed at low levels at 3 days post-transduction, significantly upregulated at 7 days post-transduction, and returned (mostly) to baseline by 15 days post-transduction. While the mouse model is very useful, it has thus far failed to replicate the immune response that has been seen in human clinical trials. Additionally, the RT-qPCR reported in the Chandler study was performed on total RNA extracted from the whole mouse retina. The *in vitro* model employed by this study allows for cell type-specific evaluation of the innate immune response, which will become important as new developments in vector design permit more precise targeting of viral vectors to this tissue. Finally, this study reported that hydroxychloroquine (HCQ) co-administration with the viral vector increased transduction efficiency both *in vitro* and *in vivo*. This increase in transduction was observed to a maximum HCQ concentration of approximately 18 μM, at which point cytotoxicity was observed. The authors postulated several potential mechanisms by which the HCQ increases transduction efficiency, but the mechanisms of action of HCQ in general are poorly understood, making further analysis difficult.

Aim 3: Interrogate the potential contribution of the RPE to the activation of retinal microglia and their translocation to the outer retina.

While innate immunity in the retina in response to viral vectors is understudied, some studies have probed the natural progression of IRDs, including a 2015 report from Zhao et al [18]. In this study, the progression of retinal degeneration in the *rd10* mouse (a model of retinitis pigmentosa with non-functional *Pde6b*, which encodes cGMP phosphodiesterase 6B, rod receptor, beta polypeptide) was evaluated at various time points. In retinitis pigmentosa, mutations disrupt the normal function of the rod photoreceptors which leads to their death. As a secondary consequence of the loss of the rod photoreceptors, cone photoreceptors are also lost [50]. Zhao and colleagues demonstrated that the retinal microglia are not present in the ONL during early stages of the disease but translocate to the outer nuclear layer as more and more photoreceptors undergo apoptosis. Per the authors, "Ramified microglia in the inner retina, sensing photoreceptor stress via unknown signals, infiltrate the outer nuclear layer…expressing markers of activation…, pro-inflammatory cytokines (e.g., IL-1β), and phagocytic molecules…" [18]. These findings indicated that, particularly in the case of the degenerative retina where photoreceptors are presenting PS or other "eat-me" signals, preventing microglia from infiltrating the ONL should greatly improve the outcomes of subretinally-injected viral gene therapies. As discussed in Section 1.2. "stressed-but-viable" photoreceptors still contribute to vision and should be spared. This study attempted to extend the results of Zhao et al. by thoroughly characterizing the secretion of chemoattractant cytokines by the RPE, potentially offering insight into the "unknown mechanisms" by which the microglia are drawn into the ONL.

1.4.1. RT-qPCR Targets and selection rationale

The following targets were selected for RT-qPCR interrogation in this study.

APOBEC3G

APOBEC3G (OMIM #607113, *22q13.1*) encodes apolipoprotein B mRNA-editing enzyme, catalytic polypeptide-like 3G (APOBEC3G), a member of the *APOBEC3* gene family of cytidine deaminases [51]. These proteins play a role in defense against retroviruses by deaminating cytosine residues in retroviral genomes to uracil residues, effectively introducing destabilizing point mutations in up to 20% of cytosine residues in the HIV-1 genome [52]. Expression of the homolog *Apobec3* in the murine retina (evaluated via whole retina RNA extraction/RT-qPCR) was upregulated by an average of approximately 6-fold in response to subretinal administration of 1 x 10^9 AAV2.GFP vector genomes [46].

BCL2L1

BCL2L1 (OMIM #600039, *20q11.21*) encodes BCL2-like 1 (BCL2L1), an anti-apoptotic protein. The BCL-2 family contains both pro- and anti-apoptotic proteins, which balance each other out under normal conditions [53]. Effects of these genes are seen when the members of this family are unbalanced (potentially because of selective upregulation of one gene). This target was selected as it was one of the genes identified by Barnes et al. [54] that is upregulated during the TLR-initiated response to virus. *BCL2L1* was therefore hypothesized to be upregulated in response to viral vectors.

BST2

BST2 (OMIM #600534, *19p13.11*) encodes bone marrow stromal cell antigen 2 (BST2, also known as tetherin). Tetherin an anti-viral protein that is induced by type I interferons [55]. When cells are infected by enveloped viruses specifically, the virus replicates itself and new viral

particles “bud” out of the cell membrane. When BST-2 is upregulated, however, it “tethers” these budding viral particles to the membrane, preventing their release and subsequent infection of neighbor cells. Wild-type viruses differ from viral vectors as viral vectors are replication deficient and do not produce new virions in transduced cells, but BST-2 was still probed for this study because it has also been found to facilitate viral entry, possibly through a “reverse tethering” mechanism [56].

CCL2

CCL2 (OMIM #158105, *17q12*) encodes chemokine, CC motif, ligand 2 (CCL2), a chemokine that modulates inflammation in the retina. CCL2 levels in the retina strongly influence the localization and activation of microglia [57]. CCL2 has been implicated in both chronic and acute inflammation in the central nervous system, and is known to increase the permeability of the blood-brain barrier, permitting leukocyte infiltration [58]. In preliminary evaluations of iPSC-RPE, CCL2 was one of the three cytokines that could be detected in culture media, along with IL6 and IL8 (data not shown).

CGAS

CGAS (OMIM #613973, *6q13*) encodes cyclic GMP-AMP synthase (cGAS), which works in concert with STING (see below) to monitor the cytosol of the cell for DNA [59]. cGAS binds to DNA which leads to the conversion of GTP and ATP to cGAMP. cGAMP then binds to STING, and the resulting signaling cascade stimulates production of type I interferons. Unlike TLR9, which differentiates between self and foreign DNA by detecting the methylation state of CpG motifs, cGAS will non-specifically detect DNA present in the cytosol. *Cgas* is one of the genes upregulated in response to AAV in the murine retina [46].

CXCL10

CXCL10 (OMIM #147310, *4q21.1*) encodes chemokine, CXC motif, ligand 10 (CXCL10). CXCL10 is also known as IP-10 or interferon-inducible 10 kDa protein. CXCL10 is an important modulator of the immune response in the CNS and can attract and stimulate many different immune cells (including T cells, B cells, and NK cells) to mount an inflammatory response [60]. This gene was recommended as a general indicator of pro-inflammatory/anti-viral response by Dr. Kai Chan, and is one of the genes upregulated in response to AAV in the murine retina [46].

FGFR4

FGFR4 (OMIM #134935, *5q35.2*) encodes fibroblast growth factor receptor 4 (FGFR4), a receptor in the FGF family. FGFR4 is a receptor for bFGF, and FGFR4 levels in primary human RPE were upregulated as part of the innate response to viral RNA through the TLR3 pathway [45], [54], [61]. Activation of the signaling cascade initiated by FGFR4 is known to be angiogenic (promotes formation of new blood vessels); angiogenesis is an issue in many retinal degenerations where the RPE is compromised, and can cause age-related macular degeneration (AMD) [45]. As a result, upregulation of *FGFR4* by viral vectors should be minimized to avoid further damage to degenerative retinas or (in the worst case) triggering an AMD phenotype.

IFITM3

IFITM3 (OMIM #605579, *11p15.5*) encodes interferon-induced transmembrane protein 3 (IFITM3). IFITM3 prevents viruses from fusing with endosomal membranes, blocking their entry into the cell [62]. There is evidence to suggest that IFITM3 is incorporated into the membrane of enveloped viruses as they bud from infected cells, limiting their infectivity. Viral vectors, however, are replication-deficient, so this mechanism of action is likely not effective against them. The exact mechanisms of action for IFITM3 are not well understood, but knockout

experiments both *in vivo* and *in vitro* reinforce the importance of IFITM3 in the anti-viral response [62].

IFNB1

IFNB1 (OMIM #147640, *9p21.3*) encodes interferon β-1 (IFNB1), one of the major Type I interferons [63]. *IFNB1* expression can be upregulated through several signaling pathways, including the pathways activated by Toll-like receptors and by cGAS. As the name "interferon" suggests, IFNB1 contributes to the anti-viral innate response by "interfering" with the viral lifecycle. When a cell has detected viral infection, the cell secretes IFNB1, which is detected by nearby cells. IFNB1 stimulates upregulation of a family of "interferon stimulated genes" (ISGs) that stimulate changes in gene expression in nearby cells [63]. These changes in gene expression either restrict/prevent viral replication (in cells that have already been infected) or increase cellular defences against viral infection (in cells that have not yet been infected).

IL1B

Interleukin 1-beta (*IL1B*, OMIM #147720, *2q14.1*) encodes interleukin 1β (IL1β), a potent pro-inflammatory cytokine that has long been used as an indicator of broad inflammation [64]. Poly(I:C) stimulated a rapid, significant increase in *IF1B* expression levels in human primary RPE. ARPE-19 cells that are exposed to IL1β downregulate expression of genes important for RPE function, including *RLBP1, RPE65,* and *RDH5* [65]. Additionally, IL1β-treated ARPE-19 demonstrate compromised barrier function and upregulate expression of IL6, IL8, and CCL2 [14].

IL6

IL6 (OMIM #147620, *7p15.3*) encodes interleukin 6 (IL6). IL6 is a pro-inflammatory cytokine that is involved in a very broad range of innate immune responses, including differentiation of B

cells and interferon-like anti-viral responses [66]. Stimulation of many different signaling pathways (including Toll-like receptors (TLRs) and other nucleic acid receptors) [66] stimulate upregulation of *IL6*. The effects of IL6 are equally broad, causing "rapid induction of an extensive range of acute phase proteins" [66]. *IL6* is significantly upregulated in primary human RPE in response to Poly(I:C) stimulation [45]. In preliminary evaluations of iPSC-RPE, IL6 was one of the three cytokines that could be detected in culture media, along with IL8 and CCL2 (data not shown).

IL8

IL8 (OMIM #146930, *4q13.3*) encodes interleukin 8 (IL8). IL8 is also known as neutrophil chemotactic factor because of the role it plays in attracting leukocytes to sites of damage or immune insult [67]. IL8 also stimulates angiogenesis through the NF-κB pathway. In preliminary evaluations of iPSC-RPE, IL8 was one of the three cytokines that could be detected in culture media, along with IL6 and CCL2 (data not shown).

NFAT5

NFAT5 (OMIM #604708, *16q22.1*) encodes the nuclear factor of activated T cells 5 (NFAT5). NFAT5 functions downstream of Toll-like receptors to facilitate the inflammatory response by altering expression levels of cytokines and chemokines, secreted structural proteins, and enzymes [68]. NFAT5 also impacts the cell cycle, although this role may be diminished in the retina and the post-mitotic photoreceptors. *NFAT5* is significantly upregulated in primary human RPE in response to Poly(I:C) stimulation [45].

RELA

RELA (OMIM #164014, *11q13.1*) encodes the RELA protooncogene, NFKB subunit (RELA, also known as the p65 NF-κB subunit). NF-κB signaling is regulated in the cytosol by IκB; in

response to insult, various signaling pathways initiate the ubiquitination and subsequent degradation of IκB [69]. When RELA is not bound to IκB, it can translocate to the nucleus where it acts as a transcription factor for many pro-inflammatory genes. *RELA* is significantly upregulated in primary human RPE in response to Poly(I:C) stimulation [45].

RSAD2

RSAD2 (OMIM #607810, *2p25.2*) encodes radical S-adenosyl methionine domain-containing protein 2, also known as virus inhibitory protein, endoplasmic reticulum-associated, interferon-inducible or "viperin". *RSAD2* expression can be upregulated in response to interferons, "double-stranded DNA, double-stranded RNA (dsRNA) analogues, LPS and multiple viruses" [70]. While broad anti-viral effects have been observed, the exact mechanism of action by which RSAD2 works is yet unclear. Interestingly, however, RSAD2 has been implicated in the disruption of geranylgeranylation [70]. RSAD2 may be of particular interest during treatment of choroideremia, which is itself the consequence of a defect in geranylgeranylation. *RSAD2* expression in primary human RPE were upregulated as part of the innate response to viral RNA through the TLR3 pathway [54].

STING

STING (OMIM #612374, *5q31.2*) encodes stimulator of interferon response cGAMP interactor 1 (STING). STING is a component of the cGAS-STING pathway; when cGAS detects cytosolic DNA, it initiates a signaling cascade that causes STING to oligomerize [59]. This oligomerization in turn initiates a cascade that ultimately results in the activation and nuclear translocation of the transcription factor IRF3, which drives IFNβ expression [59]. *Sting* is one of the genes upregulated in response to AAV in the murine retina [46].

TLR2

TLR2 (OMIM #603028, *4q31.3*) encodes Toll-like receptor 2 (TLR2). TLR2 senses the protein capsid of AAV and (as demonstrated in human liver) can drive "up-regulation of TNFα, IL-6, IL-8, and several components of the IL-1 pathway, but notably no type I IFN[s]" [71]. TLR2 involvement in the retina has not been thoroughly characterized, but was included because Kumar et al. confirmed constitutive expression of TLR2 in primary human RPE [25].

TLR3

TLR3 (OMIM #603029, *4q35.1*) encodes Toll-like receptor 3 (TLR3). TLR3 is expressed by the RPE and retinal microglia, where it detects dsRNA [72]. *TLR3* is upregulated in primary human RPE in response to Poly(I:C) stimulation [45]. TLR3 stimulation with Poly(I:C) also drives upregulation of *IL6*, *IL1B*, *TNF*, and other pro-inflammatory genes; importantly, the media from RPE treated with Poly(I:C) causes "markedly enhanced" secretion of IL6, IL-1β, and Cox2 by microglia [72]. *TLR3* is significantly upregulated in primary human RPE in response to Poly(I:C) stimulation [45].

TLR9

TLR9 (OMIM #605474, *3p21.2*) encodes Toll-like receptor 9 (TLR9), which detects unmethylated CpG motifs [73]. A high proportion of CpG motifs in vertebrate genomes (approximately 80%) are methylated, but the same motifs in bacterial, viral DNA, and viral vectors produced in bacteria are unmethylated [74]. Stimulation of TLR9 causes a response through the NF-κB pathway, leading to the upregulation of *TNF*, *IL1B*, and other pro-inflammatory genes [73]. *TLR9* is significantly upregulated in primary human RPE in response to Poly(I:C) stimulation [45], and is one of the genes upregulated in response to AAV in the murine retina [46].

2. METHODS

2.1. Culture and characterization of iPSC-derived RPE

The cells utilized in this study were RPE derived from patient normal induced pluripotent stem cells (iPSC-RPE, cell line ID "VK-WT"; gift from the lab of Dr. Vasiliki Kalatzis, Institute of Neurosciences of Montpellier, FRA). Cells were cultured on Falcon® permeable supports (PET membranes with 0.4 μm pores; Corning, Cat. No. 353090, Corning, NY) in 2.0 mL of iPSC-RPE media (0.5 mL on apical side of membrane, 1.5 mL on basal side; iPSC-RPE media composition in Table 5). Before plating, cells were removed from liquid nitrogen, thawed for 3 minutes in a 37°C water bath, then transferred dropwise into 25 mL of pre-warmed iPSC-RPE media with a pipette. Following 5 minutes of centrifugation (300 RCF), cells were re-suspended in fresh media, counted on a hemocytometer, and seeded at a density of 150,000 cells per well. Media was supplemented with 10% FBS for the first 24 hours, 5% FBS for the second 24 hours, and 1% FBS for the third 24 hours, after which serum-free media was used. Media was replaced every Monday, Wednesday, and Friday. Cells were incubated at 37˚C with 5% CO_2. Cells were kept in culture for a minimum of 30 days before treatment, with cells used for the RT-qPCR/ELISA analysis at 3 days and 7 days were kept in culture for a minimum of 2 months before treatment.

iPSC-RPE were characterized at various timepoints to monitor their progressive maturation. Media was removed from each well with a pipette and cells were gently rinsed twice (1 mL per rinse) with PBS (GE Healthcare Life Sciences, Cat. No. SH30256.01; Logan, UT). Cells were fixed via incubation in 1 mL 2% paraformaldehyde (PFA) for 20 minutes at room temperature, gently rinsed twice (1 mL per rinse) with PBST and blocked via incubation in 1 mL IFBS for 15 minutes at room temperature. Transwells were then probed (one hour, room

temperature, protected from light) with antibodies (1:50 dilution for each antibody, IFBS to a total of 400 uL per Transwell). Each well was rinsed twice (1 mL per rinse) with PBST and stained with 100 µL of 5 µM DAPI per well (5 minutes, room temperature, protected from light). The well was rinsed twice (1 mL per rinse) with PBS before the membrane was cut out of the insert and mounted on a glass slide with 30 uL of ProLong Glass (ThermoFisher Scientific, Cat. No. P36984) on each side of the membrane. Slides were left to cure overnight in a drawer (to protect them from light) at room temperature before image capture on a WaveFX spinning disk confocal microscope. Maximum intensity projections were produced and pseudocoloured with ImageJ (v2.1.0). The antibodies used for probing are detailed in Table 1.

Table 1: Antibody probes used to characterize iPSC-RPE maturation

Target	Supplier	Part Number	Conjugated Fluorophore
ZO-1	ThermoFisher Scientific, Rochester, NY	339188	Alexa Fluor 488
BEST1	Santa Cruz Biotechnology, Dallas, TX	sc-32792 AF546	Alexa Fluor 546
CLDN19		sc-365967 AF647	Alexa Fluor 647

2.2. Vector production and purification

AAV.GFP: 10 million HEK293T cells were plated on tissue culture-treated 150 mm dishes (Thermo Scientific, Cat. No. 103183, ThermoFisher Scientific, Rochester, NY) in a total of 20 mL of HEK293T media (10 total dishes). Cells were incubated overnight (37˚C, 5% CO_2) before triple transfection with transfer (pAAV.GFP; Cell BioLabs, Cat. No. AAV-400, Cell BioLabs, San Diego, CA), helper (pHelper; Cell BioLabs, Cat. No. 340402, Cell BioLabs, San Diego, CA), and rep/cap (pAAV-RC2; Cell BioLabs, Cat. No. 340201, Cell BioLabs, San Diego, CA). The mass ratio of the plasmids (transfer:helper:rep/cap) was 1:1:2, and a total of 10.5 µg of

plasmid was used to transfect each plate. The transfection reagent was 25 kDa linear polyethylenimine (PEI; Polysciences Inc., Cat. No. 23966, Polysciences Inc., Warrington, PA) in deionized water (7.5 mM, pH adjusted to 7.4 with NaOH). The "N/P ratio" (ratio of moles of nitrogen from the PEI to moles of phosphorus from the plasmid DNA) of the transfection mixtures was 40 (160 µL of 7.5 mM PEI per 10 µg of DNA), as determined by transfection optimization experiments (data not shown). To create each transfection mixture, the three plasmids were added to 150 mM NaCl, followed by dropwise addition of PEI, to a total volume of 2 mL per plate to be transfected. The conical tube containing the transfection mixture was thoroughly vortexed (>45 seconds), then incubated (20 minutes, room temperature) before dropwise addition to the 150 mm dishes of HEK293T cells. 72 hours post-transfection, cells were harvested and virus was purified with an AAVpro® Purification Kit (Takara, Cat. No. 6666, Takara Bio USA, Mountain View, CA) per the manufacturer's instructions.

The viral genomes contain a GFP transgene driven by the strong constitutive chicken β-actin (CBA) promoter.

EIAV.GFP: 10 million HEK293T cells were plated on tissue culture-treated 150 mm dishes (Thermo Scientific, Cat. No. 130183, ThermoFisher Scientific, Rochester, NY) in a total of 20 mL of HEK293T media (49 total dishes). Cells were incubated overnight (37°C, 5% CO_2) before triple transfection with transfer (pEIAV-SIN6.1 CGFPW; Addgene, Cat. No. 44171, Addgene, Watertown, MA), helper (pEV53D; Addgene, Cat. No. 44168, Addgene, Watertown, MA), and envelope (pMD.VSVG; plasmid.com, Fargo, ND) plasmids. The mass ratio of the plasmids (transfer:helper:envelope) was 2:1.8:0.7, and a total of 10 µg of plasmid was used to transfect each plate. The transfection reagent was 25 kDa linear polyethylenimine (PEI; Polysciences Inc., Cat. No. 23966, Polysciences Inc., Warrington, PA) in deionized water (7.5 mM, pH adjusted to

7.4 with NaOH). The "N/P ratio" (ratio of moles of nitrogen from the PEI to moles of phosphorus from the plasmid DNA) of the transfection mixtures was 40 (160 µL of 7.5 mM PEI per 10 µg of DNA), as determined by transfection optimization experiments (data not shown). To create each transfection mixture, the three plasmids were added to 150 mM NaCl, followed by dropwise addition of PEI, to a total volume of 2 mL per plate to be transfected. The conical tube containing the transfection mixture was thoroughly vortexed (>45 seconds), then incubated (20 minutes, room temperature) before dropwise addition to the 150 mm dishes of HEK293T cells. Dishes were gently agitated to distribute the transfection mixture before incubation (37°C, 5% CO_2). At 8 and 24 hpt, the media on each plate was aspirated to waste and replaced with 20 mL of fresh media. Plates were incubated (37°C, 5% CO_2) for an additional 48 hours before media was harvested and filtered through 0.45 µm aPES filters (Thermo Scientific, Cat. No. 165-0045, ThermoFisher Scientific, Rochester, NY). The filtration step physically removed contaminants larger than the vector, leaving behind the vector and smaller contaminants. Filtered media was ultracentrifuged (2 hours, 4°C, 19000 RPM). Supernatant was decanted to waste and ultracentrifuge bottles were inverted on paper towel for approximately 15 minutes to allow media to run off the pellet. Remaining media was wiped from ultracentrifuge bottle walls with Kimwipes™. The pellet in each tube was resuspended in 100 µL 1x PBS (GE Healthcare Life Sciences, Cat. No. SH30256.01, Logan, UT) and transferred to a 1.5 mL Eppendorf tube before being vortexed to homogenization. The vector was then further purified via high performance liquid chromatography (HPLC) to remove contaminants smaller than the vector. HPLC purification was performed by Dr. Ryan Noyce on a GE ÄKTA system with a GE Capto™ Core 700 column (Cytiva Life Sciences, Cat. No. 17548115, Global Life Sciences Solutions USA LLC, Marlborough, MA). In HPLC, the viruses (approximately 100 nm in diameter) pass

through a “column” of densely packed agarose beads. These beads have small pores on the outside that permit the entry of small contaminants, but the virus particles are too large and travel slowly through the empty spaces outside of the beads. The contaminants are then trapped inside the beads, as the agarose has been modified to be hydrophobic and positively charged to capture dyes, cell debris, extracellular nucleic acids, and other low molecular weight impurities (GE HiScreen™ Capto™ Core 700 instruction document, GE file number 28-9958-81 AF). As the vector flowed through the HPLC system, UV absorbance was measured to estimate nucleic acid concentrations in the fluid. The system then distributed 100 µL fractions of purified vector into a deep 96-well plate. These fractions were individually titred per Section 2.3. and pooled. The vector genomes contain a GFP transgene driven by the constitutive cytomegalovirus (CMV) promoter.

2.3. Vector titration

Two methods were employed to calculate the titre (concentration) of the viral vectors. The genomic titre (expressed in viral genomes per mL, vg/mL) of the AAV.GFP vector was determined with a commercially available kit, the AAVpro® Titration Kit (for Real Time PCR) (Takara, Cat. No. 6233, Takara Bio USA, Mountain View, CA). To calculate the functional titre (expressed in “transducing units per milliliter”, TU/mL) of the EIAV.GFP vector, a known volume of purified vector was added to a known number of canine osteosarcoma cells (D17, ATCC, Cat. No. CCL-183, ATCC, Manassas, VA) in 6-well tissue culture-treated plates (Thermo Scientific, Cat. No. 130184, ThermoFisher Scientific, Rochester, NY). Cells were plated in 2 mL of D17 media; approximately 16 hours later, cells were transduced with a small volume (0.5 – 10 µL) of vector. At 8 hours post-transfection (hpt), an additional 3 mL of D17 media was added per well. At 72 hpt, the media was aspirated from each well and replaced with

1 mL of 0.25% trypsin-EDTA (Gibco, Cat. No. 25200-072, ThermoFisher Scientific, Rochester, NY) per well before incubation (37°C, 5% CO_2) for 5 minutes. Each well was rinsed thoroughly with the trypsin before transferring the trypsin to a labelled 15 mL conical Falcon tube (Thermo Scientific, Cat. No. 339651, ThermoFisher Scientific, Rochester, NY). Each well was rinsed 2 additional times (1 mL of D17 media per rinse) for a total of 3 mL per well in separate conical tubes. Tubes were centrifuged (5 minutes, 400 RCF) and supernatant was aspirated to waste. Cell pellets were resuspended in 100 µL eBioscience™ Flow Cytometry Staining Buffer (Invitrogen, Cat. No. 00-4222-26, ThermoFisher Scientific, Rochester, NY), transferred to labelled 1.5 mL Eppendorf tubes. 100 µL eBioscience™ IC Fixation Buffer (Invitrogen, Cat. No. 00-8222-49, ThermoFisher Scientific, Rochester, NY) was added to each tube and tubes were incubated in the dark (60 minutes, room temperature) to fix. Tubes were centrifuged (5 minutes, 400 RCF) and supernatant was aspirated to waste. Cell pellets were resuspended in 1 mL ice-cold methanol (Fisher Scientific, Cat. No. A452-4, ThermoFisher Scientific, Rochester, NY) and stored in the -20ºC freezer for no less than 12 hours to permeabilize. Tubes were removed from the freezer and centrifuged (5 minutes, 400 RCF) and supernatant was aspirated to waste. Cell pellets were resuspended in 1 mL Flow Cytometry Staining Buffer and vortexed to rinse off the methanol. Tubes were centrifuged (5 minutes, 400 RCF) and supernatant was aspirated to waste. Cell pellets were resuspended in 100 µL Flow Cytometry Staining Buffer plus 2 µL of the appropriate antibody with conjugated AlexaFluor® 647 was added (REP-1: Santa Cruz Biotechnology, sc-23905 AF647, Santa Cruz Biotechnology, Dallas, TX; GFP: Santa Cruz Biotechnology, sc-9996 AF647, Santa Cruz Biotechnology, Dallas, TX) before being vortexed and incubated in the dark (60 minutes, room temperature). Tubes were centrifuged (5 minutes, 400 RCF) and supernatant was aspirated to waste. Cell pellets were resuspended in 1 mL Flow Cytometry Staining Buffer

and vortexed to rinse off the antibody. Tubes were centrifuged (5 minutes, 400 RCF) and supernatant was aspirated to waste. Cell pellets were resuspended in 200 µL Flow Cytometry Staining Buffer and tubes were incubated on ice before flow cytometry. Flow cytometry was completed on an Attune NxT Flow Cytometer (Invitrogen, Cat. No. A29003, ThermoFisher Scientific, Rochester, NY). Functional titre was calculated with (Equation 1):

$$\text{Titre} = \frac{\left[\frac{(\%\text{ positive cells [transduced]})-(\%\text{ positive cells [negative control]})}{100}\right][\#\text{ of cells}]}{\text{Vector volume in µL}} \quad \text{(Equation 1)}$$

2.4. Treatment summary

For the "immediate response" experiment (Section 0 treatments were applied to the wells per Table 2:

Table 2: Summary of treatments applied to iPSC-RPE for the "immediate response" experiment (0-hour, 2-hour, 4-hour, and 6-hour timepoints)

Treatment	Stock Concentration	Volume of Stock Added	Volume of PBS Added	Final Concentration (in 500 µL media)
PBS	N/A	N/A	10 µL	N/A
Poly(I:C)	8 µg/µL	1.25 µL	8.75 µL	20 µg/mL
IFNγ	1 ng/µL	10 µL	0 µL	20 ng/mL
CpG-DNA	500 µM	10 µL	0 µL	5 µM
CpG-Control	500 µM	10 µL	0 µL	5 µM

The Poly(I:C) concentration was reduced from the 100 – 500 µg/mL used in the Brosig et al. study to 20 µg/mL. Preliminary experiments (data not shown) showed that the response at this concentration was excessive, so the concentration was reduced to bring the response into a similar range to the other treatments. IFNγ concentration was selected in a similar manner. CpG-DNA and CpG-Control concentrations of 5 µM were chosen per the manufacturers' recommendations (recommended range of 1 – 5 µM).

For the "delayed response" experiment (Section 3.4. , treatments were applied to the wells per Table 3:

Table 3: Summary of treatments applied to iPSC-RPE for the "delayed response" experiment (3- and 7-day timepoints)

Treatment	Stock Concentration	Volume of Stock Added	Volume of PBS Added	Final Concentration (in 500 µL media)
PBS	N/A	N/A	25 µL	N/A
Poly(I:C)	8 µg/µL	1.25 µL	23.75 µL	20 µg/mL
IFNγ	1 ng/µL	20 µL	5 µL	40 ng/mL
AAV.GFP	3.1×10^{11} vg/mL	3.5 µL	***	MOI ≈ 1100
EIAV.GFP	1.36×10^{11} vg/mL	10 µL	15 µL	MOI ≈ 1350

***: for the "AAV.GFP" treatment, 21.5 µL of PBS added per well; for the "AAV.GFP + HCQ" treatment, 5 µL of 1.8 mM HCQ and 16.5 µL of PBS added per well (final HCQ concentration of 18 µM).

AAV.GFP and EIAV.GFP doses were limited by vector stocks and were administered at the highest possible MOI (≈1100 for AAV.GFP, ≈1350 for EIAV.GFP).

2.5. Evaluation of cytokine and chemokine production/secretion

Cytokine and chemokine secretions were measured via sandwich ELISA, conducted both in-house with commercial kits (All Invitrogen; IL-6: Cat. No. 88-7066-86, CCL2: Cat. No. 88-7399-86, CXCL10: Cat. No. CHC2363. ThermoFisher Scientific, Rochester, NY) and by Eve Technologies (IL-6, IL-8, and CCL2, custom cytokine array manufactured by MilliporeSigma; Calgary, AB). For the in-house ELISA analysis, 100 µL of media was removed from each sample at the appropriate time points, and 100 µL of fresh media was added to the well to maintain media volume. The sampled media was frozen at -20˚C (short-term) or -80˚C (long-term) until ready to be used in the ELISA assay.

Expression of cytokines, chemokines, and other inflammatory markers were measured via RT-qPCR. For primer pairs, see Table 7. RNA was first extracted from each sample with a

GeneJET RNA Purification kit (Thermo Scientific, Cat. No. K0732, ThermoFisher Scientific, Rochester, NY) following kit protocol "B. Mammalian Cultured Cells Total RNA Purification Protocol". Briefly, media was removed from the apical and basal sides of each Transwell by pipette. The apical side of each well was gently rinsed 2 times with 1 mL of DPBS per rinse. 600 µL of lysis buffer (supplemented with 20 µL of β-mercaptoethanol per kit instructions) was added to each well, and cell monolayer was removed from the Transwell via a combination of rinsing with the lysis buffer and mechanical scraping of the bottom of the Transwell with the pipette tip. The lysis buffer was then transferred to a sterile 1.5 mL Eppendorf tube, where the cells were lysed completely via a combination of vortexing and repeated aspiration by pipette. 360 µL of anhydrous ethanol was added to each lysate, and the sample was mixed via repeated aspiration by pipette (~10 times per sample). The remainder of the purification was performed according to the kit instructions, modified to elute the RNA off the column with nuclease-free water over 2 centrifugations (16000 RCF, 1', 50 µL of water per elution).

The concentration of purified RNA in each sample was determined with a colorometric plate reader (Thermo Scientific, Cat. No. 51119300, ThermoFisher Scientific, Rochester, NY) running SkanIt Software RE (Thermo Scientific, version 5.0.0.42). Samples were loaded onto a µDrop plate (Thermo Scientific, Cat. No. N12391, ThermoFisher Scientific, Rochester, NY) in duplicate (2 µL of purified RNA per replicate), along with nuclease-free water in duplicate. The average A_{260} and average A_{280} values for each sample were calculated, and the average A_{260} and A_{280} values of the blanks were subtracted. RNA concentration was then calculated via (Equation 2):

$$[\mathrm{DNA}] = \left(A_{260\ \text{average, sample}} - A_{260\ \text{average, blank}}\right) \cdot 40 \cdot 20 \qquad \text{(Equation 2)}$$

In this equation, the adjusted A_{260} is multiplied by 40 (Beer-Lambert law coefficient for RNA) and 20 (optical path adjustment for the MultiSkan Go) to give the DNA concentration in ng/µL. Approximately 500 ng (0.5 µg) of each sample was then used for first-strand (cDNA) synthesis with the RevertAid RT Reverse Transcription kit (Thermo Scientific, Cat. No. K1691, ThermoFisher Scientific, Rochester, NY). Briefly, 500 ng of RNA was added to 1 µL of 10x DNAse I reaction buffer (with $MgCl_2$), 1 µL DNAse I (RNAse-free), and nuclease-free water (to a total volume of 10 µL) in an RNAse-free tube. The tube was then gently mixed via repeated pipetting, briefly centrifuged, and incubated for 30 minutes at 37˚C on a thermocycler (Bio-Rad, Cat. No. S1000, Hercules, CA). 1 µL of 50 mM EDTA was added to each sample before another incubation on the Bio-Rad S1000 (65˚C, 10'). In each tube, 1 µL of random hexamer primer, 4 µL of 5x reaction buffer, 1 µL of RiboLock RNAse inhibitor, and 2 µL of RevertAid reverse transcriptase were added (in that order) before gentle mixing by pipetting. The samples were incubated at 25˚C (5 minutes), then 42˚C (60 minutes), then 70˚C (5 minutes). cDNA was stored at -80˚C until used in RT-qPCR reactions.

To evaluate fold-expression of target genes, RT-qPCR and the $\Delta\Delta C_T$ method were employed. Reactions were performed in MicroAmp Optical 96-well or 384-well plates (Applied Biosystems, Cat. Nos. 4346906 or 4309849 respectively, ThermoFisher Scientific, Rochester, NY). Each well contained 10 µL of Fast SYBR Green Master Mix (Applied Biosystems, Cat. No. 4385616, ThermoFisher Scientific, Rochester, NY), 0.5 µL of 10 µM forward primer, 0.5 µL of 10 µM reverse primer, 8 µL of nuclease-free water, and 1 µL of cDNA. Each well was mixed via gentle repeated pipetting, then the plate was sealed with MicroAmp clear adhesive film (Applied Biosystems, Cat. No. 4306311, ThermoFisher Scientific, Rochester, NY). Plates were centrifuged (2 minutes, 2000 RCF) before being run on an Applied Biosystems 7900HT Fast

Real-Time PCR System. Per the instructions included with the master mix, polymerase was activated with a 20 second hold at 95˚C, followed by 40 cycles of amplification and data collection (1 second denaturation at 95˚C followed by 20 seconds of annealing and extension at 60˚C). The fold expression of each gene was determined via the $\Delta\Delta C_T$ method. ΔC_T was calculated by subtracting the C_T of the housekeeping gene (*ACTB*) from the C_T of the target gene for each treatment. $\Delta\Delta C_T$ was calculated by subtracting the ΔC_T for the untreated control from the ΔC_T of the treated sample. Fold expression was calculated per (Equation 3):

$$\text{Fold expression} = 2^{-\Delta\Delta C_T} \quad \text{(Equation 3)}$$

2.6. Data visualization and statistical analysis

Data visualization and statistical analysis was performed using Microsoft Excel (v16.49) and GraphPad Prism (v9.1.1). In the short-term (0- to 6-hour) study, only one biological replicate could be completed, so no statistical analysis could be performed. In the long-term (3- to 7-day) study, simple averages of the RT-qPCR technical replicates (fold-changes in expression) or ELISA quantifications were calculated in Excel before plotting and statistical analysis was performed in Prism. For the RT-qPCR and ELISA data, pair-wise t-test comparisons of each treatment against the untreated samples were performed for each time point, assuming Gaussian distribution of the expression levels but applying Welch's correction to account for the unequal variance between samples.

3. RESULTS

3.1. iPSC-RPE in culture phenotypically resemble native RPE

After approximately 3 weeks in culture, the iPSC-RPE had organized and was positive for 4 of the 5 "P's" of functional RPE: pigmented, polarized, post-mitotic, and polygonal (the 5th

"P", "phagocytic activity", was not evaluated) [47]. Polarization was confirmed via the "pumping" of fluid from the apical side of the cells to the basal side, resulting in pockets of media underneath the monolayer (data not shown). The cells ceased to divide, maintaining a monolayer, and assumed a polygonal morphology due to the formation of tight junctions, as confirmed via the localization of the mature tight junction protein Claudin-19 (CLDN19) at cell-cell boundaries. Cells also began to express bestrophin (a marker of RPE) after approximately 20 days (Figure 1). Taken together, the gross morphology and immunofluorescence data suggest that the iPSC-RPE phenotypically resemble native RPE.

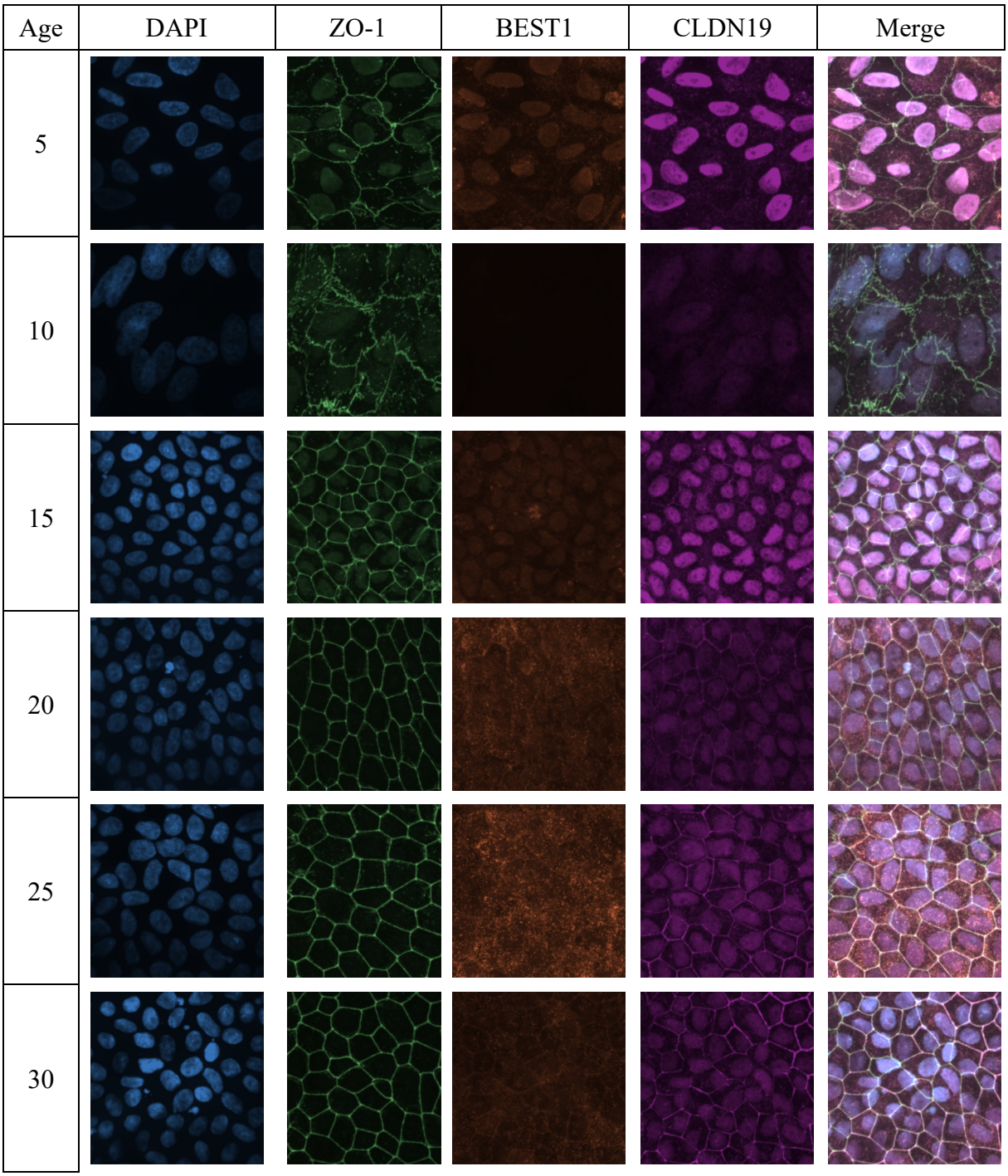

Figure 1. Progressive maturation and of iPSC-RPE in culture. iPSC-RPE quickly express ZO-1, which localizes to cell boundaries. At approximately 15 days post-plating, they begin to increase expression of BEST1 (an RPE-specific gene) and CLDN19 (an indicator of mature tight junctions). By 30 days post-plating, the iPSC-RPE have formed mature tight junctions with CLDN19 localizing at the cell boundaries. Macroscopically (not shown), the RPE have also developed pigment by the 30-day post-plating time point and are actively pumping fluid from their apical side to their basal side.

3.2. Titration of AAV and EIAV vectors

AAV.GFP: According to the AAVpro® Titration Kit (for Real Time PCR) kit (comparing the vector produced in the lab to a serial dilution of standardized genomes) the AAV.GFP vector had a purified concentration of 3.11×10^{11} vg/mL.

EIAV.GFP: Each fraction of HPLC-purified EIAV vector was titred per section 2.3. Briefly, each 100 µL fraction from the HPLC column was used to transduce 2 wells of D17 cells for 72 hours (one well with 1 µL of purified vector and the other with 5 µL of purified vector). Each well was fixed, permeabilized, and probed with α-GFP antibody (Santa Cruz Biotechnology, sc-9996 AF647, Santa Cruz Biotechnology, Dallas, TX) before flow cytometry. The percentage of GFP+ cells for each well was determined, and the functional titre (TU/mL) was calculated. In the two "blank" (untreated) samples, 0.126% and 0.142% of cells were gated as "GFP+", giving an average false positive rate of 0.134% (equivalent to 804 cells for a well containing 600,000 cells). This false positive rate was subtracted from each subsequent measurement for treated wells. The calculated functional titre from each fraction is listed in Table 4.

Table 4: Transducing unit per milliliter (TU/mL) calculations for HPLC-purified EIAV.GFP

EIAV.GFP Fraction (from HPLC)	Vector Volume (µL)	% GFP+ cells	# Positive cells (assuming 600,000 per well)	Minus Blank (804 cells)	TU/mL (x 10^7)	Average TU/mL (x 10^7)
F1	1	0.500	3000	2196	0.22	0.13
	5	0.500	3000	2196	0.04	
F2	1	0.554	3324	2520	0.25	0.16
	5	0.752	4512	3708	0.07	
F3	1	0.901	5406	4602	0.46	0.46
	5	4.000	24000	23196	0.46	
F4	1	2.717	16302	15498	1.55	1.60
	5	13.913	83478	82674	1.65	
F5	1	4.046	24276	23472	2.35	1.96
	5	13.268	79608	78804	1.58	
F6	1	5.522	33132	32328	3.23	2.88
	5	21.161	126996	126162	2.52	
F7	1	4.768	28608	27804	2.78	2.54
	5	19.217	115302	114498	2.29	
F8	1	3.640	21840	21036	2.10	1.96
	5	15.335	92010	91206	1.82	
F9	1	3.688	22128	21324	2.13	1.95
	5	14.824	88944	88140	1.76	
F10	1	2.754	16524	15720	1.57	1.50
	5	12.011	72006	71262	1.43	

To maximize the quantity of vector recovered while maintaining the highest possible titre, fractions F4 through F10 were pooled; this combined a total of 1.44 x 10^7 TU's in 700 µL of PBS for a final functional titre of 2.06 x 10^7 TU/mL (Figure 2).

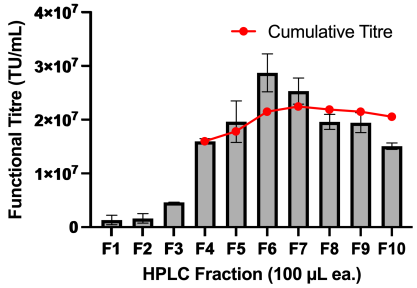

Figure 2: Fractional and cumulative titres of EIAV.GFP, as determined by flow cytometry. Fractions F1, F2, and F3 were excluded from the final "pooled" vector stock, as they added significant volume (100 µL) of low-titre vector, decreasing the final concentration. Although the peak concentration of vector could be achieved by combining fewer fractions, fractions F4 through F10 were selected to maximize the number of transducing units while maintaining a high vector concentration.

3.3. Immediate response (0 hours – 6 hours post-treatment) of iPSC-RPE to cytokines/TLR agonist treatment

iPSC-RPE were treated per Table 2 and were harvested at 2-, 4-, or 6-hours post-treatment. The strongest responses were observed after treatment with Poly(I:C), which caused notable upregulation of many genes, including >10-fold increases in *CXCL10*, *IFNB1*, *IL6*, *IL8*, *RSAD2*, and *TLR3* for at least one timepoint each (Figure 3). While this experiment was only completed once to conserve wells of mature iPSC-RPE (making statistical analysis impossible), each timepoint represents a distinct biological replicate. These data show that, in response to Poly(I:C), the iPSC-RPE rapidly upregulate innate immunity and antiviral genes. IFNγ stimulated apparent upregulation of *CXCL10* and *RSAD2*, while the CpG-DNA and CpG-Control oligonucleotides did not stimulate any obvious differences in gene expression.

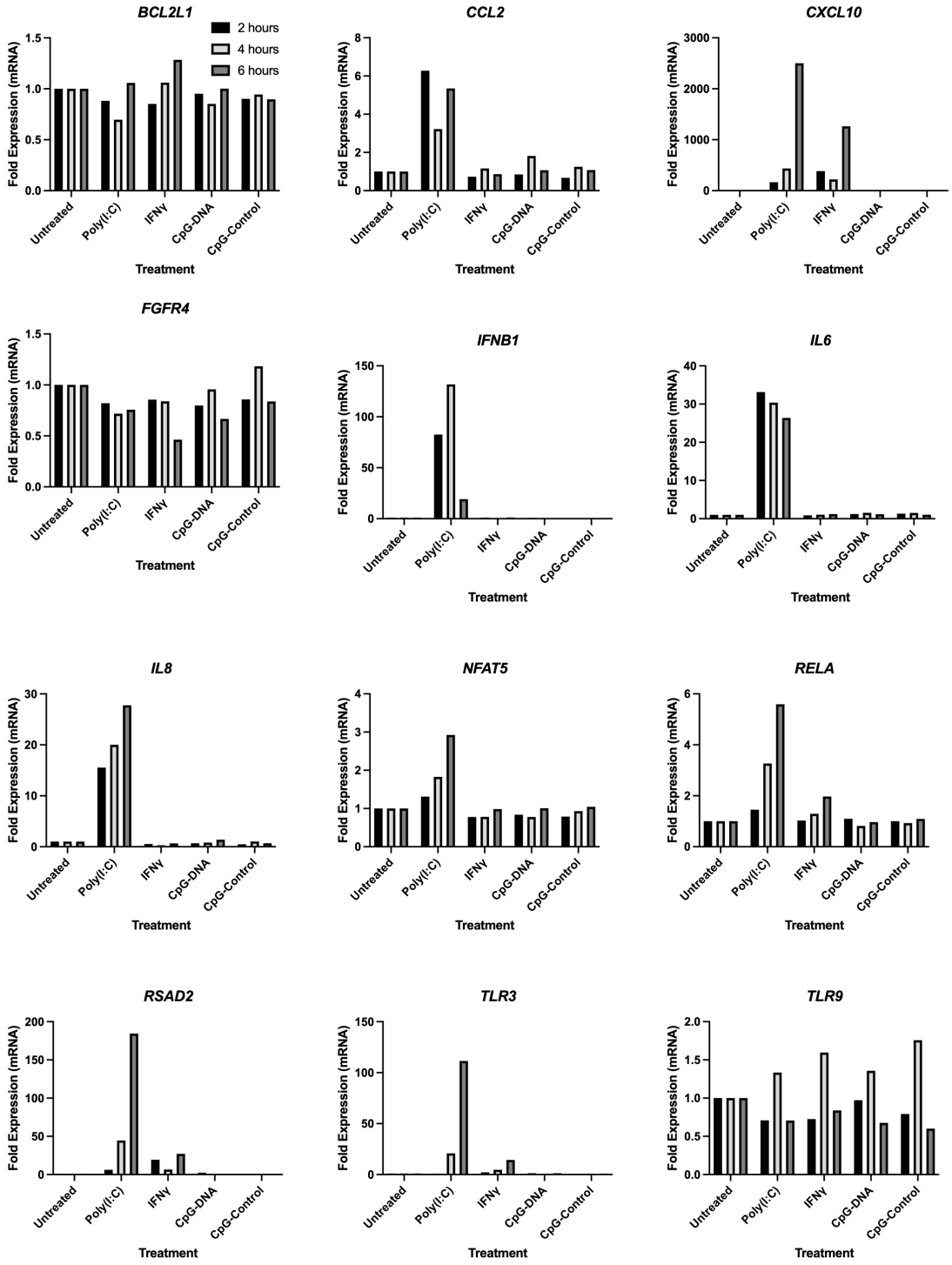

Figure 3: RT-qPCR analysis of innate immunity and anti-viral response genes early (2-6 hours) post-treatment. Many of the innate immunity and anti-viral genes were upregulated rapidly after treatment, but the statistical significance of the increase could not be calculated, as only one biological replicate of each condition/time point was collected to preserve wells of mature iPSC-RPE.

3.4. Delayed response (3 days and 7 days post-treatment) of iPSC-RPE to cytokines, TLR agonists, and viral vectors

iPSC-RPE were treated per Table 3. For each well, media was sampled for ELISA analysis after 3 days of incubation in untreated media (giving an "untreated baseline" for each well), 3 days post-treatment, or (if applicable) 7 days post-treatment. At the designated evaluation time (3 days or 7 days post-treatment), the well was harvested via lysis and RNA was purified, followed by reverse transcription into cDNA and RT-qPCR analysis of various indicators of innate immune activation and antiviral response.

3.4.1. RT-qPCR

The 3- and 7-day post-treatment RT-qPCR results are summarized in Figure 4. Most of the vector treatments failed to stimulate a statistically significant response in the iPSC-RPE, which was likely due to the low transduction efficiencies that were achieved.

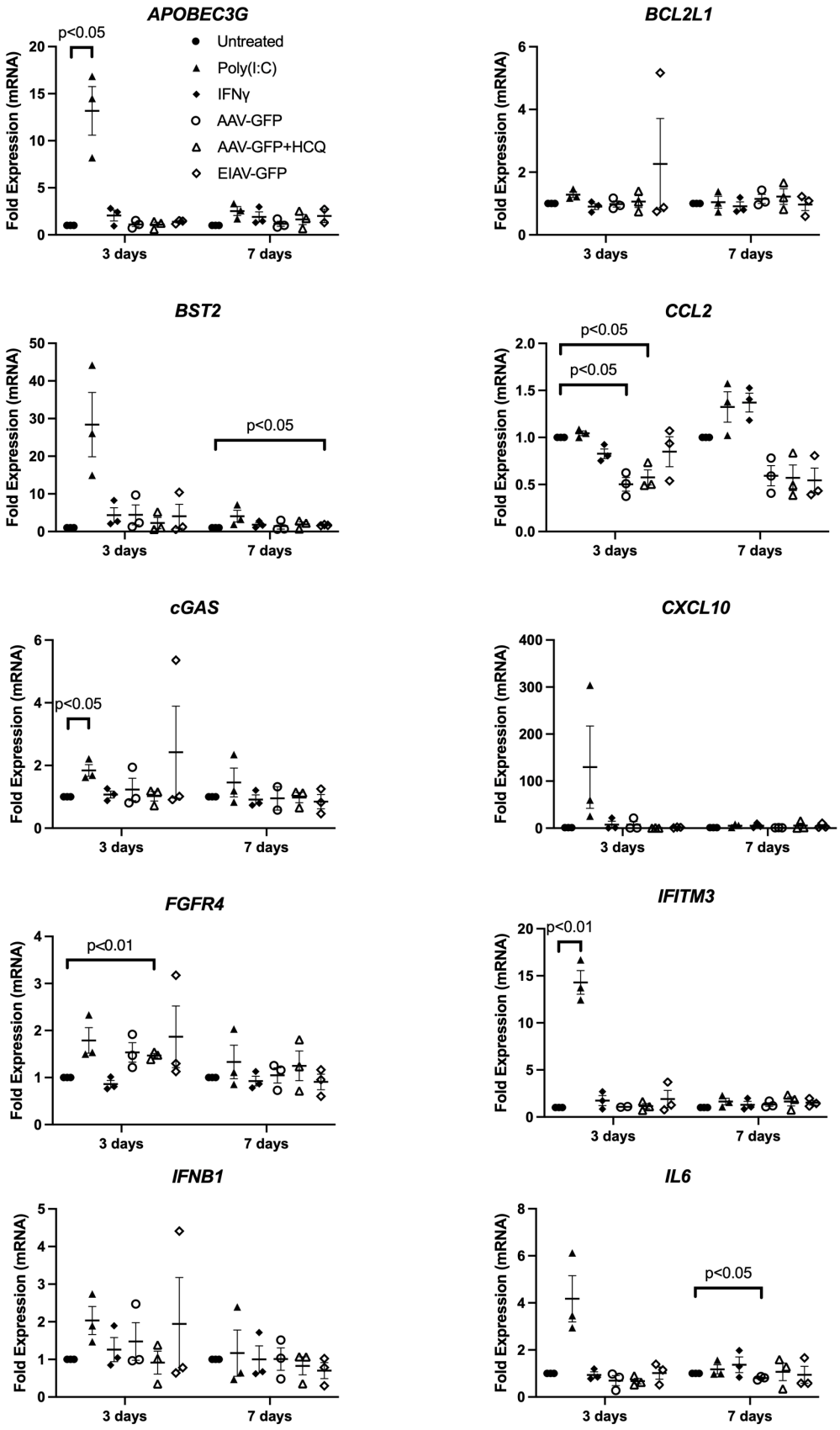
APOBEC3G
p<0.05
Untreated
Poly(I:C)
IFNγ
AAV-GFP
AAV-GFP+HCQ
EIAV-GFP
Fold Expression (mRNA)
3 days
7 days
BCL2L1
BST2
p<0.05
CCL2
p<0.05
p<0.05
cGAS
p<0.05
CXCL10
FGFR4
p<0.01
IFITM3
p<0.01
IFNB1
IL6
p<0.05

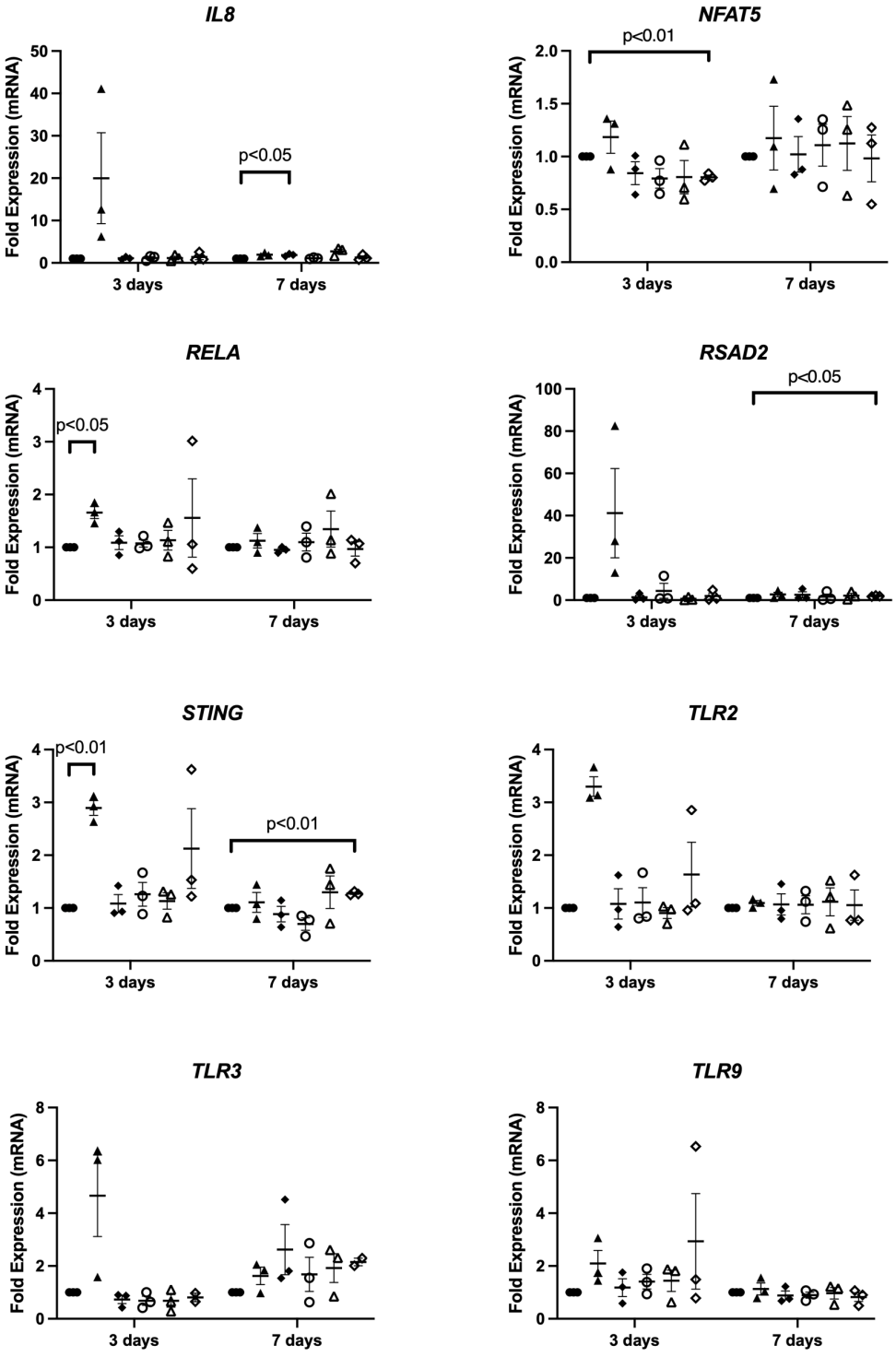

Figure 4: Fold-expression of mRNA for various cytokines, chemokines, and innate immunity genes in response to 3 days or 7 days of treatment with Poly(I:C), IFNγ, AAV.GFP vector (with or without hydroxychloroquine), or EIAV.GFP vector.

RT-qPCR, when analyzed using the $\Delta\Delta C_T$ method, can only differentiate changes in gene expression. As a result, the absolute quantification of transduction levels in each sample cannot be determined via $\Delta\Delta C_T$, as "untransduced" samples do not express GFP transcripts and therefore cannot provide a baseline. In this study, however, differences in gene expression between the AAV.GFP and AAV.GFP + HCQ samples can be measured, with HCQ considered as the "treatment". Average fold changes in GFP mRNA expression levels between these treatments are shown in Figure 5. While the differences were small and did not reach statistical significance, there appears to be a trend toward increased transduction caused by addition of 18 μM HCQ, in agreement with the findings of Xue et al. [46].

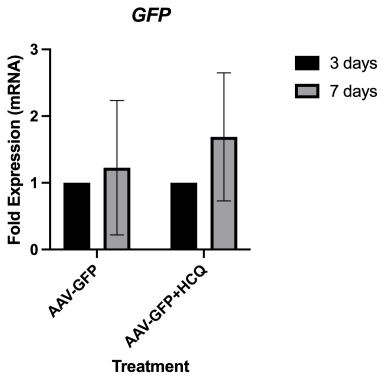

Figure 5: Differences in *GFP* expression between wells treated with and without 18 μM hydroxychloroquine (HCQ). Although very few cells were GFP+ because of either treatment, addition of HCQ appeared to cause a trend toward increased transduction, especially at 7 days post-treatment (n=3 per treatment).

3.4.2. ELISA

Average concentrations of IL6, IL8, and CCL2 from harvested cell culture media are shown in Figure 6.

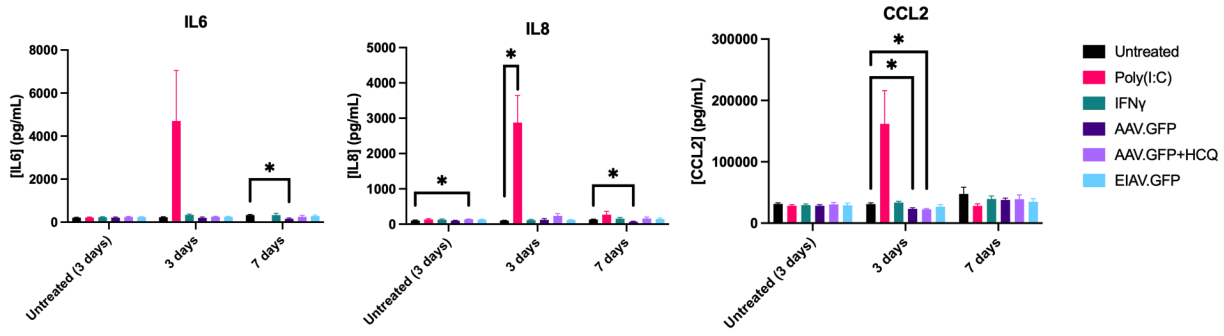

Figure 6: IL6, IL8, and CCL2 concentrations in iPSC-RPE media in response to various viral and pro-inflammatory stimuli. iPSC-RPE media was harvested after 3 days of culture (untreated), 3 days post-treatment, and 7 days post-treatment. * indicates $p<0.05$ (pair-wise t-test with Welch's correction).

Like the results of the RT-qPCR analysis, treatment with viral vectors had minimal impact on the average cytokine levels in the cell culture media, likely a result of the low transduction achieved. Although increases in all three cytokines were observed after treatment with Poly(I:C), only IL8 (3 days post-treatment) was increased to a statistically significant level. To interrogate these data further (even though the changes were not statistically significant), the measurements for each well were plotted to evaluate trends separately. Surprisingly, treatment with the vector decreased IL8 secretion at the 7-day time-point, and treatment with the vector ± HCQ decreased CCL2 secretion at the 3-day time-point.

IL6: The 3- and 7-day post-treatment ELISA results (IL6) are summarized in Figure 7. The wells treated with Poly(I:C) or IFNγ demonstrated increased IL6 secretion during the first 3 days of treatment (compared to 3 days without treatment) before decreasing after the media change at the 3-day timepoint. Wells treated with AAV.GFP + HCQ or EIAV.GFP, conversely, tended to demonstrate increased IL6 secretion during the 3-to-7-day period. Treatment with AAV.GFP alone had a negligible effect on IL6 secretion. Of all the treatments, Poly(I:C) stimulated the

greatest increase in IL6 secretion, while the effects of IFNγ and vector treatments were much more subdued.

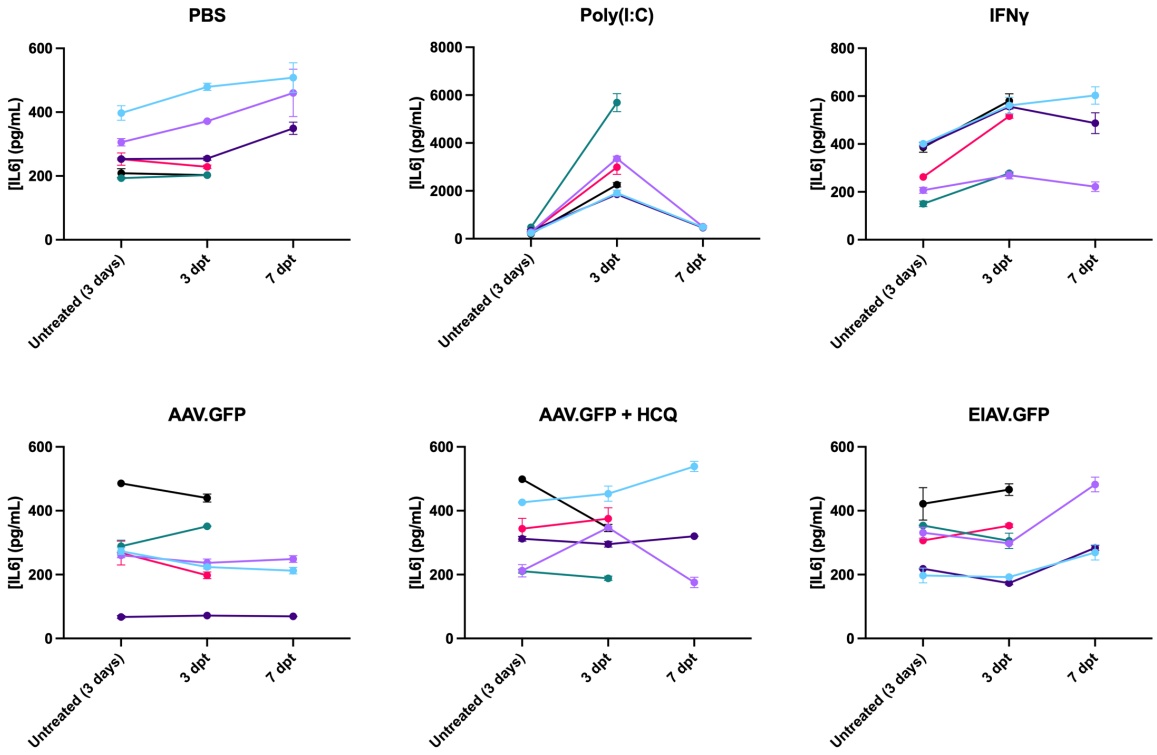

Figure 7: IL6 levels in cell media after 3 days of no treatment, 3 days of treatment, and (if applicable) 7 days of treatment. Each different color represents one well of iPSC-RPE, which was sampled at 2 or 3 different timepoints.

IL8: The 3- and 7-day post-treatment ELISA results (IL8) are summarized in Figure 8. Like the IL6 findings, wells treated with Poly(I:C) demonstrated increased IL8 secretion during the first 3 days of treatment (compared to 3 days without treatment) before decreasing after the media change at the 3-day timepoint. IFNγ and AAV.GFP (± HCQ) treatment had nearly no effect on the iPSC-RPE. EIAV.GFP stimulated an apparent increase in IL8 secretion in a manner like IL6, where IL8 levels remained constant (or decreased) during the first 3 days of treatment, but then increased during the 3- to 7-day period. Of all the treatments, Poly(I:C) stimulated the greatest

increase in IL8 secretion, while the effects of IFNγ and vector treatments were much more subdued.

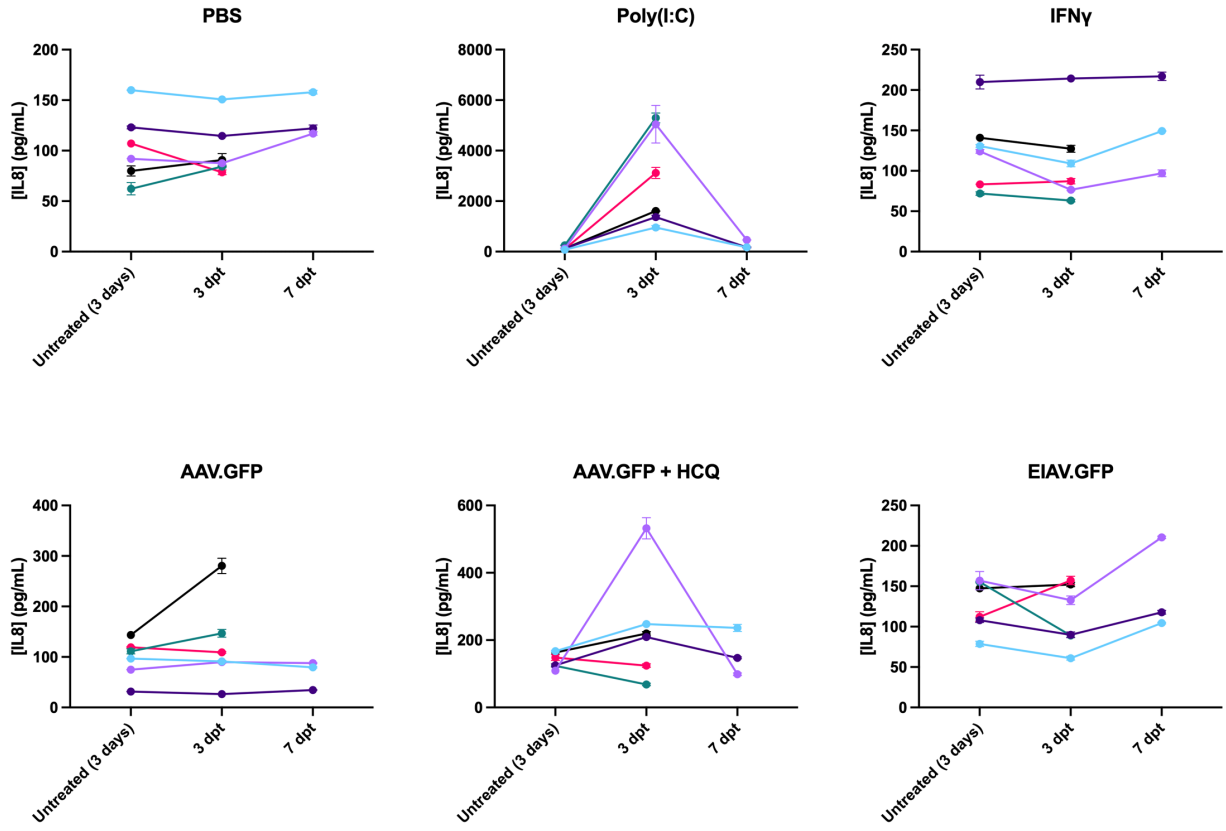

Figure 8: IL8 levels in cell media after 3 days of no treatment, 3 days of treatment, and (if applicable) 7 days of treatment. Each different color represents one well of iPSC-RPE, which was sampled at 2 or 3 different timepoints.

CCL2: The 3- and 7-day post-treatment ELISA results (CCL2) are summarized in Figure 9. Like the IL6 and IL8 findings, wells treated with Poly(I:C) demonstrated increased CCL2 secretion during the first 3 days of treatment (compared to 3 days without treatment) before decreasing after the media change at the 3-day timepoint. IFNγ treatment had nearly no effect on the iPSC-RPE. All viral vectors (± HCQ) stimulated an apparent increase in CCL2 secretion in a manner like IL6, where CCL2 levels remained constant (or decreased) during the first 3 days of treatment, but then increased during the 3- to 7-day period. Of all the treatments, Poly(I:C)

stimulated the greatest increase in IL8 secretion, while the effects of IFNγ and vector treatments were more subdued.

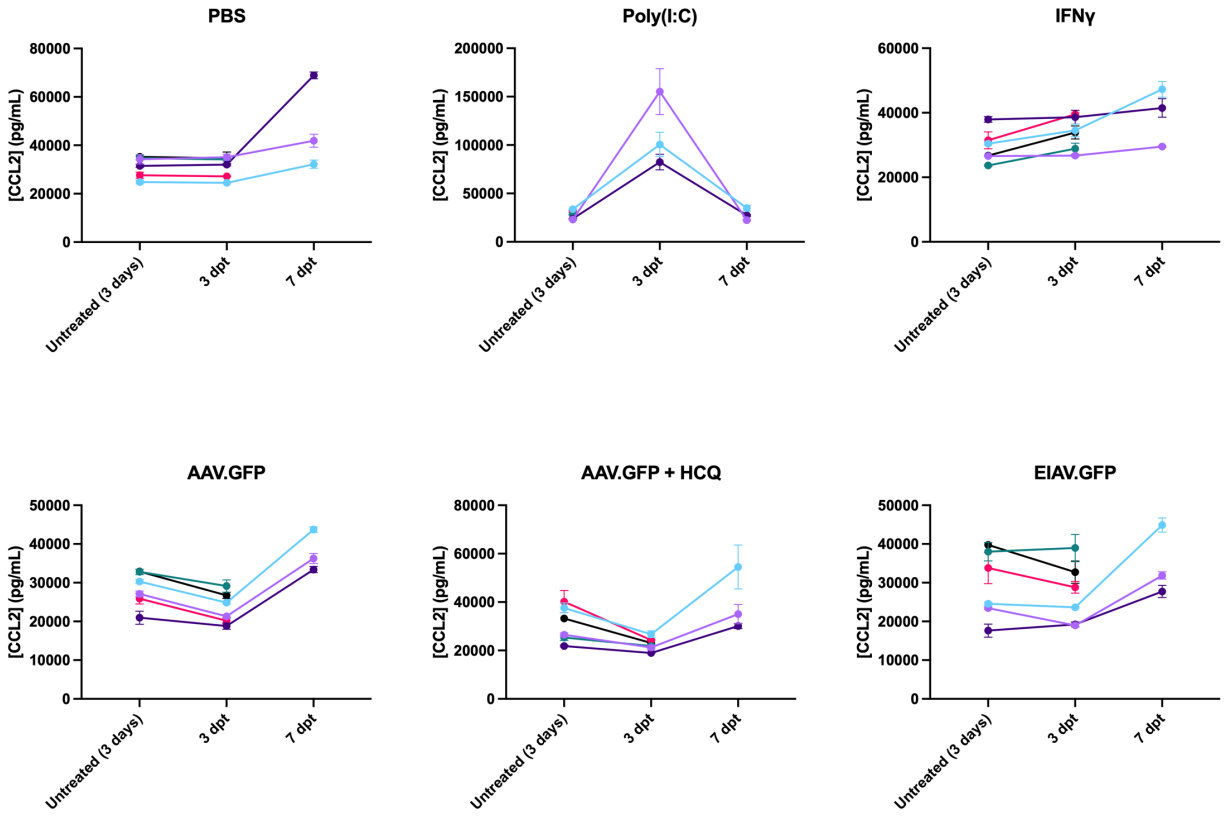

Figure 9: CCL2 levels in cell media after 3 days of no treatment, 3 days of treatment, and (if applicable) 7 days of treatment. Each different color represents one well of iPSC-RPE, which was sampled at 2 or 3 different timepoints.

4. Discussion

4.1. Ocular gene therapy vectors offer the possibility of long-term cures for inherited retinal disorders

Viral ocular gene therapies offer patients with many hereditary retinal disorders hope for treatments that were previously considered impossible. Patients are understandably excited, as these developing therapies offer the hope of preserved vision, decreased visits to their

ophthalmologist for repeated treatments or injections, and the possibility of treating their children before the disease presents itself. While this excitement is certainly justified, early clinical trial results have somewhat dampened patient and physician enthusiasm. The most successful clinical trials to-date led to FDA and Health Canada approvals for LUXTURNA® (voretigene neparvovec-ryzl) for the treatment of LCA2. More ocular gene therapies will almost certainly be approved now in the wake of the LUXTURNA® approval.

The excitement around ocular gene therapies (and gene therapies in general) has led to significant research efforts, as seen by the 65+ clinical trials currently listed on ClinicalTrials.gov that are evaluating ocular gene therapy vectors. Very few studies (clinical or pre-clinical), however, have successfully predicted and mitigated serious adverse events. Animal models have long been the gold standard for pre-clinical evaluation of new therapies, but the increasing number of human clinical trials that are reporting inflammatory response to viral vectors seems to suggest that the animal models do not accurately recapitulate the response of humans experiencing ongoing retinal degeneration. As researchers have circled back to probe the potential causes of immune response to vectors more thoroughly in pre-clinical and *in vitro* work and efficacy of mitigation measures, the field will develop a more nuanced picture of the true impacts of these therapies.

4.2. iPSC-RPE response to immune stimuli and viral vectors

In this study, expression of several genes/gene products involved in the innate immune response were assayed via ELISA or RT-qPCR in the short-term (2 to 6 hours) or long term (3 to 7 days) after exposing iPSC-RPE to cytokines, TLR agonists, or viral vectors. The strongest responses were seen in the samples that were treated with 20 µg/mL Poly(I:C), primarily in the short-term study. This is in agreement with the work of Kumar et al. [25], who reported that

TLR3 is constitutively expressed in human primary RPE cells. Poly(I:C) is an analogue of viral RNA and an agonist of TLR3, so the dramatic pro-inflammatory response of the iPSC-RPE to Poly(I:C) confirms that iPSC-RPE also constitutively express TLR3 and can detect viral RNA, and that iPSC-RPE mount a pro-inflammatory response quickly upon detecting viral RNA. This is important to recognize as more viral vectors enter clinical trials for use in the retina, even though few trials utilize RNA-based vectors. IFNγ also appeared to stimulate a rapid pro-inflammatory response, although the observable effect of IFNγ at 20 ng/mL was limited to *CXCL10*, *RSAD2*, and *TLR3*.

In the 3- to 7-day experiment, very few collected datapoints met statistical significance, limiting the ability to draw conclusions regarding their immunogenicity in iPSC-RPE. The most likely cause of this shortcoming was the low transduction efficiencies that were observed; in each treated well, an estimated <1% of iPSC-RPE were successfully transduced/expressed the GFP transgene 7 days post-treatment (data not shown). At these low levels of transduction, significant variability between samples and subsequent high variability of readouts is to be expected. Some of the trends observed in the data merit further study. RT-qPCR is a highly sensitive method to detect changes in gene expression, but it is limited by the homogenization of the sample that occurs during RNA extraction. Although each individual cell may dramatically alter gene expression in response to transduction, the mRNA from transduced cells contributes to the "bulk" RNA from the entire well, effectively "diluting" the effect and confounding the results. Further, wells were treated with Poly(I:C) and EIAV.GFP (both of which should stimulate an immune response through the TLR3 pathway), but only Poly(I:C) produced a detectable response. Further study is certainly required to determine the cause of the low transduction efficiency. This is likely due to an insufficient multiplicity of infection (MOI); to

successfully transduce cells, there must be a sufficiently high ratio of viral particles to target cells. While both the AAV.GFP and EIAV.GFP vectors were able to easily transduce D17 cells during vector titration, transducing iPSC-RPE cells was much more difficult, requiring large quantities of high-titre vector. When vector is detected during transduction, the cells not only try to limit the vector within the cell itself, but also secrete innate immune signals that are detected by nearby bystander cells, which in turn stimulates an anti-viral response, preventing successful transduction. As a result, the low transduction efficiencies observed likely not only affected the data by contributing relatively little to the harvested mRNA, but by actively preventing transduction of nearby cells. In the ELISA data, treatment with the vector decreased IL8 secretion at the 7-day time-point, and treatment with the vector ± HCQ decreased CCL2 secretion at the 3-day time-point. This is the opposite of the hypothesized effect of the treatment but is still likely due to a poor signal-to-noise ratio in the data. Even though these datapoints reached statistical significance ($p<0.05$, t-test with Welch's correction), I hypothesize that the differences observed were due to factors other than the treatments as the transduction efficiency was negligible. With that in mind, this phenomenon certainly merits further investigation and future studies should consider that a suppressive effect is possible.

5. Conclusions and Future directions

There are several ways that the issues identified in Section 4.2. could be addressed in future work, producing a more accurate representation of the *in vivo* innate immune response of iPSC-RPE. Transduction efficiency could be addressed in at least two ways: increasing the multiplicity of infection by adding more virus particles per well, or by selectively enriching transduced cells before RT-qPCR. One of the key lessons learned from this study is that the "lab-scale" production of high titre viral vectors can be labour-intensive and expensive. In future

experiments, vectors produced in industrial facilities will be used to maximize the number and concentration of viral particles. This would also add traceability to the experiment, provided that the manufacturer followed GLP or GMP protocols. Alternatively, because the transgene is GFP, it would be possible to separate the transduced cells from the untransduced cells via FACS before RNA extraction, allowing for the true effects of transduction to be measured. If high enough transduction cannot be achieved (limiting the amount of RNA that can be purified), single-cell RNAseq could be utilized.

The limitations on the data analysis due to low transduction efficiency prevent making broad conclusions around the innate immune response of iPSC-RPE to viral vectors, and there is much yet to study. The experiments described here will be repeated with larger stimuli. Additionally, the crosstalk between the retinal pigment epithelium and retinal microglia merits investigation. In future experiments, iPSC-RPE with and without microglia co-culture will interrogate ways that the two cell types interact with each other and how those interactions can specifically and transiently be disrupted to increase transduction efficiency while minimizing the immune response. Finally, the long-term implications of successful transduction must be investigated. As an example, Cepko et al. [75] reported that AAV-driven transgene expression in the RPE causes toxicity; in fact, even viral vectors that had a null transgene driven by an RPE-specific promoter (producing no protein) caused toxicity in the RPE. Future studies will also need to consider the possibility of anti-transgene responses for gene replacement therapy. These types of responses are akin to vaccinations: the introduction of a new, “non-self” protein is interpreted in patient cells as an infection. For patients with loss-of-function mutations, it is unlikely that wild-type transgenes are identified as “foreign” in cells as the transgene is similar to the mutated gene. Patients with null mutations, however, may be completely naïve to therapeutic

transgenes, potentially resulting in transgene fragments being loaded on MHC Class I molecules and subsequent clearance of transduced cells by CD8+ T cells [29]. The extent to which this anti-transgene response occurs is unknown but will need to be thoroughly investigated to ensure that sufficient mitigation strategies are incorporated into the treatment protocol.

As the field of ocular gene therapy with viral vectors continues to mature and therapies become more refined, the effects of innate immune responses to these vectors in the retina will become increasingly important. The *CHM* mutations that cause choroideremia disrupt vesicular trafficking and signaling within each cell; the most effective therapies would therefore re-introduce wild-type *CHM* into every RPE and photoreceptor cell. To increase the proportion of the photoreceptors and RPE that are transduced, vectors are injected into the subretinal space. This procedure creates a retinal detachment in a retina that is already experiencing the deleterious effects of the IRD itself. While overall transduction can be increased with increasing vector dosage, the increased immune response in the retina (due to both the increased vector concentration and the retinal detachment) will likely mitigate the therapeutic effects of the treatment somewhat. Based on the available literature and the findings of this study, I hypothesize that the RPE plays an important role in the innate immune response to viral gene therapy vectors in the retina by detecting viral particles (through Toll-like receptors and other unknown mechanisms) and producing pro-inflammatory and anti-viral molecules. I also hypothesize that pharmaceuticals, modifications to the viral genome, or other methods to block the innate immune response will improve the safety profile of these vectors and allow for increased transduction efficiency.

The degenerative retina must be treated carefully to protect the post-mitotic photoreceptors. As discussed, the *rd10* mouse model suggests that the translocation of activated

retinal microglia to the ONL is pathogenic because "stressed-but-viable" photoreceptors are mistakenly phagocytosed. These "stressed-but-viable" photoreceptors present "eat-me" signals to the microglia, marking them for primary phagocytosis. It is highly likely that the photoreceptors in other IRDs (including choroideremia) experience similar stress and present these "eat-me" signals, so prevention of microglial translocation should be a common goal of the therapies for these diseases. Indeed, modulation of microglia has proven preventative in several studies. In the Zhao et al. study, retinal microglia were ablated by creating a mouse line that expressed tamoxifen-inducible diphtheria toxin under the control of the CX3CR1 promoter, which is specific to microglia. In *rd10* (*Pde6b*$^{-/-}$) mice without microglia, the ONL thickness was spared and the response to visual stimuli (as measured by ERG) was improved [24]. Furthermore, a study report by Zhang et al. utilized a mouse line with RP-causing mutations in *Pde6a* (rod phosphodiesterase). These mice were manipulated such that tamoxifen treatment caused Cre-driven expression of the wild-type *Pde6a* gene. Activation of retinal microglia and phagocytosis of photoreceptors was observed during disease progression, but genetic rescue with tamoxifen rapidly restored normal (non-diseased) microglia localization and morphology [76]. Finally, a recent study from Vijayasarathy et al. [77] reported a similar reduction in inflammatory response and improved retinal structure in a mouse model of X-linked retinoschisis (XLRS) following treatment with AAV8.RS1 (correcting the genetic defect that causes retinoschisis). Importantly, their RNAseq analysis revealed microglial pro-inflammatory gene expression was reduced following genetic rescue. Retinoschisin (RS1) is secreted by photoreceptors into the subretinal space, so therapeutic benefit could be achieved without complete transduction of the retina, or by transduction of non-photoreceptor cells, so long as they secrete the transgenic protein. This could permit lower doses of vector to be utilized when compared to treatments for choroideremia, as

the *CHM* gene product REP-1 is not secreted, and therefore only transduced cells are genetically rescued.

This study did not address gene therapy strategies other than gene replacement. As mentioned, choroideremia is a prime candidate for gene replacement; as an X-linked gene, males only have one copy of *CHM*, and the disease is exclusively caused by the lack of a single functional copy of the gene. Disorders with different etiologies, however, may require much different strategies. As an example, retinitis pigmentosa can be caused by mutations in over 50 different genes [50]. Developing gene replacement vectors for each of those genes would be exceedingly expensive and time-consuming. Treatments for these types of disorders are more amenable to gene-independent strategies, where the transgene or the target of gene editing is different from the gene with the causative lesion. Yu et al. recently utilized an AAV-based CRISPR/Cas9 system to disrupt the *Nrl* gene in rods as a possible gene-independent RP therapy [78]. The *Nrl* gene is important in determining and maintaining rod fate, so disruption of *Nrl* in the developed retina causes rods to take on cone-like characteristics. The authors hypothesize that the development of cone-like characteristics reduced the deleterious impact of the rod-specific mutation, allowing the rods to survive longer and preventing secondary loss of cones. In three mouse models of RP (all with different causative mutations), disruption of *Nrl* led to improved retinal function and reduced rod loss, suggesting that the therapy was truly independent of the causative mutation. This strategy (and other CRISPR/Cas9-based strategies) do have their own set of risks, however. Cas9 can create off-target double-stranded breaks if RNA other than the supplied guide RNA is utilized. The probability of off-target cuts increases as Cas9 expression is increased, or as Cas9 is expressed for longer periods of time; as a result, Cas9 expression will likely have to be tightly regulated to minimize the risks of unintentional

off-target damage. Additionally, this study did not address gene delivery methods other than viral-mediated gene transfer. In viral-mediated gene transfer, researchers have started with wild-type viruses and attempted to remove as much of the viral genome as possible while modifying the remaining DNA or RNA and structural proteins to minimize immunogenicity. Non-viral gene therapy strategies utilize the opposite approach; the vectors (typically DNA plasmids) are constructed from the ground up, and only the required genetic elements are included to minimize immunogenicity [79]. This is an appealing concept, but these vectors are still in the "proof-of-concept" stage and one of the biggest challenges to implementing these vectors has to do with plasmid delivery *in vivo*. Viruses were selected as gene therapy vectors because they have evolved in nature to be very efficient at delivering genetic material into cells. From an evolutionary perspective, it makes sense that naked DNA is not readily taken up by our cells; DNA is relatively stable in our environments, and indiscriminate uptake of DNA could have unpredictable and likely deleterious effects. There are a number of very efficient transfection methods that can be used for *ex vivo* transfections of patient cells, including chemical transfections with PEI or lipid-based transfection reagents, nucleofection, or nanoparticles (liposome-based, solid-lipid, niosome, polymer-based, and lipopeptide-based, among others), as reviewed by Toualbi et al [79]. For diseases like choroideremia, however, *ex vivo* therapy is not a feasible option. Delivery of non-viral vectors to cells *in vivo* poses an interesting challenge, because the effects of the plethora of transfection reagents on these cells is currently unknown. In the future, it is highly likely that non-viral gene therapy vectors completely supplant viral vectors, but the timeline of this shift is currently unknown, and the newer delivery methods will need to undergo significant pre-clinical work and interrogation in clinical trials to ensure their safety profile is acceptable.

Taken together, the literature and this study suggest that we have an incomplete knowledge of the innate immune response of the RPE (and the retina in general) after treatment with viral gene therapy vectors. Preliminary studies have demonstrated preservation of photoreceptors via genetic ablation of retinal microglia, complete genetic rescue in a conditional mouse model, or vector-driven expression of secreted proteins, but none of these methods improve upon the existing experimental therapies for choroideremia. Gene therapy (and gene therapy for hereditary retinal disorders in particular) remains an extremely promising field of study, even though recent reports from both pre-clinical investigations and clinical trials have demonstrated that much work is yet to be done in understanding the immunogenicity of viral vectors. Although this has dampened enthusiasm for these technologies somewhat, it is important that the scientific community remains resilient and continues to develop novel solutions. As more and more of the barriers to safe, effective ocular gene therapies are elucidated and consequently overcome, more cures for hereditary blindness will become reality.

Table 5: iPSC-RPE media composition

Component	Concentration	Manufacturer	Manufacturer Part Number	Volume (mL) per 1L of Media
MEM α	1x	Gibco	12571063	932.70
FBS	20x	Gibco	A3160701	50.00
N-2 Supplement	100x	Gibco	17502001	10.00
Hydrocortisone	50 μM	Sigma-Aldrich	H6909	1.10
Taurine	50 mg/mL	Sigma-Aldrich	T0625	5.00
T_3	20 ng/mL	Sigma-Aldrich	T5516	0.70
Gentamicin	50 mg/mL	Gibco	15750060	0.50

Table 6: Complete RPE media composition

Component	Concentration	Manufacturer	Manufacturer Part Number	Volume (mL) per 1L of Media
KnockOut DMEM	1x	Gibco	10829018	769
KnockOut Serum Replacement	5x	Gibco	10828028	200
GlutaMAX	100x	Gibco	35050061	10
Non-Essential Amino Acids	100x	Gibco	11140050	10
β-mercaptoethanol	1000x	Bio-Rad	1610710	1
Penicillin/Streptomycin	100x	Gibco	15140122	10

Table 7: Primer sequences for PCR/RT-qPCR

Gene Target	Direction	Primer Sequence	Source
IL6	Forward	5'-TAC CCC CAG GAG AAG ATT CC-3'	Brosig et al. [45]
	Reverse	5'-TTT TCT GCC AGT GCC TCT TT-3'	
IL8	Forward	5'- ACT GAG AGT GAT TGA GAG TGG AC-3'	Tsai et al. [80]
	Reverse	5'- AAC CCT CTG CAC CCA GTT TTC-3'	
CCL2	Forward	5'-CCC CAG TCA CCT GCT GTT AT-3'	Brosig et al. [45]
	Reverse	5'-TGG AAT CCT GAA CCC ACT TC-3'	
TLR3	Forward	5'GCT GGA AAA TCT CCA AGA GC-3'	Brosig et al. [45]
	Reverse	5'-CTT CCA ATT GCG TGA AAA C-3'	
TLR9	Forward	5'-CAG CAG CTC TGC AGT ACG TC-3'	Brosig et al. [45]
	Reverse	5'-AAG GCC AGG TAA TTG TCA CG-3'	
TNF	Forward	5'- AAC CTC CTC TCT GCC ATC AA-3'	Brosig et al. [45]
	Reverse	5'- CCA AAG TAG ACC TGC CCA GA-3'	
IL1B	Forward	5'-GGG CCT CAA GGA AAA GAA TC-3'	Brosig et al. [45]
	Reverse	5'-TTC TGC TTG AGA GGT GCT GA-3'	
CXCL10	Forward	5'-GGT GAG AAG AGA TGT CTG AAT CC-3'	OriGene Cat. No. HP205421
	Reverse	5'- GTC CAT CCT TGG AAG CAC TGC A-3'	
RELA	Forward	5'- ATG GCT TCT ATG AGG CTG AG-3'	Brosig et al. [45]
	Reverse	5'- GTT GTT GTT GGT CTG GAT GC-3'	
NFAT5	Forward	5'- TCA CCA TCA TCT TCC CAC CT-3'	Brosig et al. [45]
	Reverse	5'- CTG CAA TAG TGC ATC GCT GT-3'	
RSAD2	Forward	5'- CCA GTG CAA CTA CAA ATG CGG C-3'	OriGene Cat. No. HP216708
	Reverse	5'- CGG TCT TGA AGA AAT GGC TCT CC-3'	
HPRT1	Forward	5'- CCT GGC GTC GTG ATT AGT GAT-3'	Dr. Lance Doucette
	Reverse	5'- AGA CGT TCA GTC CTG TCC ATA A-3'	
CFH	Forward	5'- CAG CAG TAC CAT GCC TCA GA-3'	Brosig et al. [45]
	Reverse	5'- GGA TGC ATC TGG GAG TAG GA-3'	
IFNB1	Forward	5'- CTT GGA TTC CTA CAA AGA AGC AGC-3'	OriGene Cat. No. HP205913
	Reverse	5'- TCC TCC TTC TGG AAC TGC TGC A-3'	
FGFR4	Forward	5'- AAC ACC GTC AAG TTC CGC TGT C-3'	OriGene Cat. No. HP205766
	Reverse	5'- CAT CAC GAG ACT CCA GTG CTG A-3'	
BCL2L1	Forward	5'- GCC ACT TAC CTG AAT GAC CAC C-3'	OriGene Cat. No. HP234144
	Reverse	5'-AAC CAG CGG TTG AAG CGT TCC T-3'	
ACTB	Forward	5'- CAT GTA CGT TGC TAT CCA GGC-3'	Dr. Lance Doucette
	Reverse	5'- CTC CTT AAT GTC ACG CAC GAT-3'	

Table 8: Fold-expression of RT-qPCR target genes following 3- and 7-day treatment with Poly(I:C), IFNγ, AAV.GFP (± HCQ), and EIAV.GFP

		3 days		7 days	
Treatment	**RT-qPCR Target Gene**	**Fold Expression**	**P-value (compared to untreated)**	**Fold Expression**	**P-value (compared to untreated)**
Poly(I:C) (20 µg/mL)	*APOBEC3G*	13.18	**0.042148**	2.533	0.081882
	BCL2L1	1.284	0.088331	1.043	0.841464
	BST2	28.40	0.084780	4.078	0.186273
	CCL2	1.044	0.223873	1.325	0.182044
	cGAS	1.841	**0.046272**	1.457	0.423622
	CXCL10	129.7	0.279586	5.194	0.181453
	FGFR4	1.789	0.100982	1.333	0.449150
	IFITM3	14.30	**0.008805**	1.640	0.208760
	IFNB1	2.034	0.109598	1.167	0.810872
	IL6	4.174	0.084221	1.178	0.453156
	IL8	19.99	0.218682	1.953	0.061302
	NFAT5	1.183	0.353278	1.174	0.621018
	RELA	1.657	**0.028693**	1.126	0.455248
	RSAD2	41.19	0.197436	2.681	0.244350
	STING	2.895	**0.005457**	1.107	0.625145
	TLR2	3.300	**0.006448**	1.094	0.182060
	TLR3	4.661	0.141076	1.626	0.199161
	TLR9	2.096	0.156369	1.129	0.628181
IFNγ (20 ng/mL)	*APOBEC3G*	2.056	0.206639	1.915	0.227104
	BCL2L1	0.902	0.418139	0.911	0.590138
	BST2	4.388	0.232433	1.824	0.247007
	CCL2	0.827	0.077034	1.371	0.065888
	cGAS	1.074	0.574265	0.914	0.621101
	CXCL10	7.625	0.450040	5.240	0.300907
	FGFR4	0.861	0.214353	0.925	0.548073
	IFITM3	1.074	0.291300	1.327	0.215744
	IFNB1	1.261	0.501834	1.002	0.995677
	IL6	0.939	0.688451	1.370	0.379036
	IL8	1.102	0.626019	1.869	**0.036567**

	NFAT5	0.843	0.282700	1.020	0.914289
	RELA	1.088	0.565937	0.953	0.293749
	RSAD2	1.357	0.739000	2.505	0.406806
	STING	1.086	0.659284	0.884	0.510526
	TLR2	1.079	0.809317	1.068	0.763988
	TLR3	0.732	0.227796	2.622	0.230071
	TLR9	1.181	0.647754	0.885	0.567721
3.5 µL (1.085 x 10^9 vgs) AAV2.GFP	*APOBEC3G*	1.116	0.666545	1.172	0.578421
	BCL2L1	0.984	0.885932	1.147	0.412789
	BST2	4.422	0.325348	1.429	0.639814
	CCL2	0.502	**0.020518**	0.593	0.063662
	cGAS	1.234	0.580977	0.951	0.916887
	CXCL10	7.434	0.458328	0.888	0.448481
	FGFR4	1.535	0.121448	1.048	0.796020
	IFITM3	1.748	0.294809	1.296	0.491579
	IFNB1	1.477	0.440045	1.009	0.978396
	IL6	0.697	0.292306	0.804	**0.043140**
	IL8	1.158	0.662541	1.098	0.383840
	NFAT5	0.793	0.153125	1.107	0.642543
	RELA	1.076	0.397107	1.099	0.616935
	RSAD2	4.403	0.438163	1.640	0.660049
	STING	1.260	0.369184	0.698	0.126190
	TLR2	1.104	0.748133	1.061	0.753212
	TLR3	0.685	0.209826	1.684	0.402109
	TLR9	1.407	0.281745	0.896	0.457094
3.5 µL (1.085 x 10^9 vgs) AAV2.GFP + 18 µM HCQ	*APOBEC3G*	1.086	0.766516	1.635	0.361922
	BCL2L1	1.062	0.774062	1.221	0.464612
	BST2	2.255	0.483855	1.909	0.292154
	CCL2	0.576	**0.033351**	0.571	0.087562
	cGAS	1.022	0.899838	0.977	0.900424
	CXCL10	0.402	0.237874	5.665	0.441213
	FGFR4	1.468	0.009353	1.250	0.511325
	IFITM3	1.155	0.624210	1.649	0.304900
	IFNB1	0.915	0.806057	0.829	0.546531
	IL6	0.678	0.104362	1.070	0.869601
	IL8	1.164	0.724066	2.715	0.085046

	NFAT5	0.806	0.342618	1.124	0.674238
	RELA	1.135	0.542604	1.346	0.418497
	RSAD2	0.653	0.530767	2.112	0.408345
	STING	1.133	0.480448	1.300	0.433608
	TLR2	0.905	0.451913	1.118	0.699521
	TLR3	0.682	0.311659	1.922	0.231829
	TLR9	1.440	0.390969	0.969	0.898359
10 µL (1.360 x 10^9 vgs) EIAV.GFP	*APOBEC3G*	1.390	0.078026	2.016	0.386270
	BCL2L1	2.262	0.476829	0.968	0.882162
	BST2	4.046	0.439017	1.688	0.018368
	CCL2	0.849	0.443219	0.544	0.073726
	cGAS	2.425	0.433781	0.846	0.569643
	CXCL10	1.560	0.432484	4.642	0.335443
	FGFR4	1.867	0.316952	0.907	0.629982
	IFITM3	1.910	0.421844	1.518	0.166511
	IFNB1	1.944	0.524644	0.702	0.296337
	IL6	1.018	0.951459	0.944	0.891007
	IL8	1.380	0.585948	1.285	0.51867
	NFAT5	0.8038	0.010484	0.982	0.942457
	RELA	1.557	0.530661	0.970	0.843419
	RSAD2	1.956	0.572317	1.967	**0.022796**
	STING	2.125	0.274707	1.276	**0.004686**
	TLR2	1.634	0.408739	1.054	0.867548
	TLR3	0.810	0.449233	2.153	0.079957
	TLR9	2.935	0.397197	0.8225	0.403522

LITERATURE CITED

[1] R. H. Masland, "The fundamental plan of the retina," *Nat. Neurosci.*, vol. 4, no. 9, pp. 877–886, 2001, doi: 10.1038/nn0901-877.

[2] A. Nowrouzi, H. Glimm, C. von Kalle, and M. Schmidt, "Retroviral vectors: Post entry events and genomic alterations," *Viruses*, vol. 3, no. 5, pp. 429–455, 2011, doi: 10.3390/v3050429.

[3] F. Willermain *et al.*, "Origins and consequences of hyperosmolar stress in retinal pigmented epithelial cells," *Front. Physiol.*, vol. 5 MAY, no. May, pp. 1–8, 2014, doi: 10.3389/fphys.2014.00199.

[4] A. Reichenbach and A. Bringmann, "Glia of the human retina," *Glia*, vol. 68, no. 4, pp. 768–796, 2020, doi: 10.1002/glia.23727.

[5] J. van den Hurk *et al.*, "Molecular basis of choroideremia (CHM): Mutations involving the rab escort protein-1 (REP-1) gene," *Hum. Mutat.*, vol. 9, no. 2, pp. 110–117, 1997, doi: 10.1002/(SICI)1098-1004(1997)9:2<110::AID-HUMU2>3.0.CO;2-D.

[6] D. Dalkara, O. Goureau, K. Marazova, and J.-A. Sahel, "Let There Be Light: Gene and Cell Therapy for Blindness," *Hum. Gene Ther.*, vol. 27, no. 2, pp. 134–147, 2016, doi: 10.1089/hum.2015.147.

[7] F. P. M. Cremers, S. A. Armstrong, M. C. Seabra, M. S. Brown, and J. L. Goldstein, "REP-2, a Rab escort protein encoded by the choroideremia-like gene," *J. Biol. Chem.*, vol. 269, no. 3, pp. 2111–2117, 1994, doi: 10.1161/01.CIR.37.5.680.

[8] A. Rak, O. Pylypenko, A. Niculae, K. Pyatkov, R. S. Goody, and K. Alexandrov, "Structure of the Rab7:REP-1 complex: Insights into the mechanism of Rab prenylation and choroideremia disease," *Cell*, vol. 117, no. 6, pp. 749–760, 2004, doi:

10.1016/j.cell.2004.05.017.

[9] M. I. Patrício, A. R. Barnard, K. Xue, and R. E. MacLaren, “Choroideremia: molecular mechanisms and development of AAV gene therapy,” *Expert Opin. Biol. Ther.*, vol. 18, no. 7, pp. 807–820, 2018, doi: 10.1080/14712598.2018.1484448.

[10] I. J. Crane and J. Liversidge, “Mechanisms of leukocyte migration across the blood-retina barrier,” *Semin. Immunopathol.*, vol. 30, no. 2, pp. 165–177, 2008, doi: 10.1007/s00281-008-0106-7.

[11] D. Dalkara *et al.*, “Inner limiting membrane barriers to aav-mediated retinal transduction from the vitreous,” *Mol. Ther.*, vol. 17, no. 12, pp. 2096–2102, 2009, doi: 10.1038/mt.2009.181.

[12] S. Sugita, “Role of ocular pigment epithelial cells in immune privilege,” *Arch. Immunol. Ther. Exp. (Warsz).*, vol. 57, no. 4, pp. 263–268, 2009, doi: 10.1007/s00005-009-0030-0.

[13] L. J. Rizzolo, “Development and Role of Tight Junctions in the Retinal Pigment Epithelium,” *Int. Rev. Cytol.*, vol. 258, no. 07, pp. 195–234, 2007, doi: 10.1016/S0074-7696(07)58004-6.

[14] T. Abe, E. Sugano, Y. Saigo, and M. Tamai, “Interleukin-1β and barrier function of retinal pigment epithelial cells (ARPE-19): Aberrant expression of junctional complex molecules,” *Investig. Ophthalmol. Vis. Sci.*, vol. 44, no. 9, pp. 4097–4104, 2003, doi: 10.1167/iovs.02-0867.

[15] J. V. Forrester, H. Xu, L. Kuffová, A. D. Dick, and P. G. McMenamin, “Dendritic cell physiology and function in the eye,” *Immunol. Rev.*, vol. 234, no. 1, pp. 282–304, 2010, doi: 10.1111/j.0105-2896.2009.00873.x.

[16] M. Karlstetter, S. Ebert, and T. Langmann, “Microglia in the healthy and degenerating

retina: Insights from novel mouse models," *Immunobiology*, vol. 215, no. 9–10, pp. 685–691, 2010, doi: 10.1016/j.imbio.2010.05.010.

[17] Y. Okunuki, R. Mukai, E. A. Pearsall, G. Klokman, D. Husain, and D. Park, "Microglia inhibit photoreceptor cell death and regulate immune cell infiltration in response to retinal detachment," pp. 1–10, 2018, doi: 10.1073/pnas.1719601115.

[18] L. Zhao *et al.*, "Microglial phagocytosis of living photoreceptors contributes to inherited retinal degeneration," *EMBO Mol. Med.*, vol. 7, no. 9, pp. 1179–1197, 2015, doi: 10.15252/emmm.201505298.

[19] M. Wang, W. Ma, L. Zhao, R. N. Fariss, and W. T. Wong, "Adaptive Müller cell responses to microglial activation mediate neuroprotection and coordinate inflammation in the retina Adaptive Müller cell responses to microglial activation mediate neuroprotection and coordinate inflammation in the retina," vol. 173, no. December, 2011.

[20] J. Neumann *et al.*, "Microglia Cells Protect Neurons by Direct Engulfment of Invading Neutrophil Granulocytes: A New Mechanism of CNS Immune Privilege," *J. Neurosci.*, vol. 28, no. 23, pp. 5965–5975, 2008, doi: 10.1523/JNEUROSCI.0060-08.2008.

[21] G. P. Lewis, C. S. Sethi, K. M. Carter, D. G. Charteris, and S. K. Fisher, "Microglial cell activation following retinal detachment: a comparison between species.," *Mol. Vis.*, vol. 11, no. January, pp. 491–500, 2005, [Online]. Available: http://www.ncbi.nlm.nih.gov/pubmed/16052164.

[22] T. Hisatomi *et al.*, "Clearance of apoptotic photoreceptors: Elimination of apoptotic debris into the subretinal space and macrophage-mediated phagocytosis via phosphatidylserine receptor and integrin αvβ3," *Am. J. Pathol.*, vol. 162, no. 6, pp. 1869–1879, 2003, doi: 10.1016/S0002-9440(10)64321-0.

[23] G. C. Brown and J. J. Neher, “Microglial phagocytosis of live neurons,” *Nat. Rev. Neurosci.*, vol. 15, no. 4, pp. 209–216, 2014, doi: 10.1038/nrn3710.

[24] L. Zhao *et al.*, “Microglial phagocytosis of living photoreceptors contributes to inherited retinal degeneration,” *EMBO Mol. Med.*, vol. 7, no. 9, pp. 1179–1197, 2015, doi: 10.15252/emmm.201505298.

[25] M. V. Kumar, C. N. Nagineni, M. S. Chin, J. J. Hooks, and B. Detrick, “Innate immunity in the retina: Toll-like receptor (TLR) signaling in human retinal pigment epithelial cells,” *J. Neuroimmunol.*, vol. 153, no. 1–2, pp. 7–15, 2004, doi: 10.1016/j.jneuroim.2004.04.018.

[26] G. M. Barton and R. Medzhitov, “Toll-like receptor signaling pathways,” *Science (80-.).*, vol. 300, no. 5625, pp. 1524–1525, 2003, doi: 10.1126/science.1085536.

[27] P. Colella, G. Ronzitti, and F. Mingozzi, “Emerging Issues in AAV-Mediated In Vivo Gene Therapy,” *Mol. Ther. - Methods Clin. Dev.*, vol. 8, no. March, pp. 87–104, 2018, doi: 10.1016/j.omtm.2017.11.007.

[28] R. J. Samulski and N. Muzyczka, “AAV-mediated gene therapy for research and therapeutic purposes,” *Annu. Rev. Virol.*, vol. 1, no. 1, pp. 427–451, 2014, doi: 10.1146/annurev-virology-031413-085355.

[29] G. L. Rogers, A. T. Martino, G. V. Aslanidi, G. R. Jayandharan, A. Srivastava, and R. W. Herzog, “Innate immune responses to AAV vectors,” *Front. Microbiol.*, vol. 2, no. SEP, pp. 1–10, 2011, doi: 10.3389/fmicb.2011.00194.

[30] I. Trapani, “Adeno-associated viral vectors as a tool for large gene delivery to the retina,” *Genes (Basel).*, vol. 10, no. 4, 2019, doi: 10.3390/genes10040287.

[31] M. I. Patricio, A. R. Barnard, H. O. Orlans, M. E. McClements, and R. E. MacLaren,

"Inclusion of the Woodchuck Hepatitis Virus Posttranscriptional Regulatory Element Enhances AAV2-Driven Transduction of Mouse and Human Retina," *Mol. Ther. - Nucleic Acids*, vol. 6, no. March, pp. 198–208, 2017, doi: 10.1016/j.omtn.2016.12.006.

[32] A. T. Martino and D. M. Markusic, "Immune Response Mechanisms against AAV Vectors in Animal Models," *Mol. Ther. - Methods Clin. Dev.*, vol. 17, no. June, pp. 198–208, 2020, doi: 10.1016/j.omtm.2019.12.008.

[33] K. Binley *et al.*, "Transduction of photoreceptors with equine infectious anemia virus lentiviral vectors: Safety and biodistribution of stargen for stargardt disease," *Investig. Ophthalmol. Vis. Sci.*, vol. 54, no. 6, pp. 4061–4071, 2013, doi: 10.1167/iovs.13-11871.

[34] P. A. Campochiaro *et al.*, "Lentiviral Vector Gene Transfer of Endostatin/Angiostatin for Macular Degeneration (GEM) Study," *Hum. Gene Ther.*, vol. 28, no. 1, pp. 99–111, 2017, doi: 10.1089/hum.2016.117.

[35] T. Hirsch *et al.*, "Regeneration of the entire human epidermis using transgenic stem cells," *Nature*, vol. 551, no. 7680, pp. 327–332, 2017, doi: 10.1038/nature24487.

[36] K. T. Woodard, K. J. Liang, W. C. Bennett, and R. J. Samulski, "Heparan Sulfate Binding Promotes Accumulation of Intravitreally Delivered Adeno-associated Viral Vectors at the Retina for Enhanced Transduction but Weakly Influences Tropism," *J. Virol.*, vol. 90, no. 21, pp. 9878–9888, 2016, doi: 10.1128/JVI.01568-16.

[37] K. Kataoka *et al.*, "Macrophage- and RIP3-dependent inflammasome activation exacerbates retinal detachment-induced photoreceptor cell death," *Cell Death Dis.*, vol. 6, no. 4, pp. e1731-10, 2015, doi: 10.1038/cddis.2015.73.

[38] S. J. Shelby, P. S. Angadi, Q. D. Zheng, J. Yao, L. Jia, and D. N. Zacks, "Hypoxia inducible factor 1α contributes to regulation of autophagy in retinal detachment," *Exp. Eye*

Res., vol. 137, pp. 84–93, 2015, doi: 10.1016/j.exer.2015.06.016.

[39] J. Xie *et al.*, "Tumor necrosis factor-alpha regulates photoreceptor cell autophagy after retinal detachment," *Sci. Rep.*, vol. 7, no. 1, pp. 1–11, 2017, doi: 10.1038/s41598-017-17400-3.

[40] F. F. Reichel *et al.*, "Humoral immune response after intravitreal but not after subretinal aav8 in primates and patients," *Investig. Ophthalmol. Vis. Sci.*, vol. 59, no. 5, pp. 1910–1915, 2018, doi: 10.1167/iovs.17-22494.

[41] Q. Li *et al.*, "Intraocular route of AAV2 vector administration defines humoral immune response and therapeutic potential.," *Mol. Vis.*, vol. 14, no. September 2008, pp. 1760–9, 2008, [Online]. Available: http://www.pubmedcentral.nih.gov/articlerender.fcgi?artid=2559816&tool=pmcentrez&rendertype=abstract.

[42] I. S. Dimopoulos *et al.*, "Two-Year Results After AAV2-Mediated Gene Therapy for Choroideremia: The Alberta Experience," *Am. J. Ophthalmol.*, vol. 193, pp. 130–142, Sep. 2018, doi: 10.1016/j.ajo.2018.06.011.

[43] K. Xue *et al.*, "Beneficial effects on vision in patients undergoing retinal gene therapy for choroideremia," *Nat. Med.*, vol. 24, no. 10, pp. 1507–1512, 2018, doi: 10.1038/s41591-018-0185-5.

[44] J. W. B. Bainbridge *et al.*, "Long-Term Effect of Gene Therapy on Leber's Congenital Amaurosis," *N. Engl. J. Med.*, vol. 372, no. 20, pp. 1887–1897, 2015, doi: 10.1056/NEJMoa1414221.

[45] A. Brosig, H. Kuhrt, P. Wiedemann, L. Kohen, A. Bringmann, and M. Hollborn, "Gene expression regulation in retinal pigment epithelial cells induced by viral RNA and

viral/bacterial DNA.," *Mol. Vis.*, vol. 21, no. August, pp. 1000–16, 2015, [Online]. Available: http://www.pubmedcentral.nih.gov/articlerender.fcgi?artid=4554413&tool=pmcentrez&rendertype=abstract.

[46] L. C. Chandler *et al.*, "Enhancement of Adeno-Associated Virus-Mediated Gene Therapy Using Hydroxychloroquine in Murine and Human Tissues," *Mol. Ther. - Methods Clin. Dev.*, vol. 14, no. September, pp. 77–89, 2019, doi: 10.1016/j.omtm.2019.05.012.

[47] F. Mazzoni, H. Safa, and S. C. Finnemann, "Understanding photoreceptor outer segment phagocytosis: Use and utility of RPE cells in culture," *Exp. Eye Res.*, vol. 126, pp. 51–60, 2014, doi: 10.1016/j.exer.2014.01.010.

[48] W. Samuel *et al.*, "Appropriately differentiated ARPE-19 cells regain phenotype and gene expression profiles similar to those of native RPE cells," *Mol. Vis.*, vol. 23, no. 66–xxx, pp. 60–89, 2017, doi: 10.1016/j.devcel.2016.01.012.

[49] S. Reichman *et al.*, "From confluent human iPS cells to self-forming neural retina and retinal pigmented epithelium," *Proc. Natl. Acad. Sci. U. S. A.*, vol. 111, no. 23, pp. 8518–8523, 2014, doi: 10.1073/pnas.1324212111.

[50] S. P. Daiger, L. S. Sullivan, and S. J. Bowne, "Genes and mutations causing retinitis pigmentosa," *Clin. Genet.*, vol. 84, no. 2, pp. 132–141, 2013, doi: 10.1111/cge.12203.

[51] B. Mangeat, P. Turelli, G. Caron, M. Friedli, L. Perrin, and D. Trono, "Broad antiretroviral defence by human APOBEC3G through lethal editing of nascent reverse transcripts," *Nature*, vol. 424, no. 6944, pp. 99–103, 2003, doi: 10.1038/nature01709.

[52] B. R. Cullen, "Role and Mechanism of Action of the APOBEC3 Family of Antiretroviral Resistance Factors," *J. Virol.*, vol. 80, no. 3, pp. 1067–1076, 2006, doi:

10.1128/jvi.80.3.1067-1076.2006.

[53] J. T. Opferman and A. Kothari, “Anti-apoptotic BCL-2 family members in development,” *Cell Death Differ.*, vol. 25, no. 1, pp. 37–45, 2018, doi: 10.1038/cdd.2017.170.

[54] B. J. Barnes, J. Richards, M. Mancl, S. Hanash, L. Beretta, and P. M. Pitha, “Global and distinct targets of IRF-5 and IRF-7 during innate response to viral infection,” *J. Biol. Chem.*, vol. 279, no. 43, pp. 45194–45207, 2004, doi: 10.1074/jbc.M400726200.

[55] D. T. Evans, R. Serra-Moreno, R. K. Singh, and J. C. Guatelli, “BST-2/tetherin: a new component of the innate immune response to enveloped viruses,” *Trends Microbiol.*, vol. 18, no. 9, pp. 388–396, Sep. 2010, doi: 10.1016/j.tim.2010.06.010.

[56] K. Viswanathan, M. S. Smith, D. Malouli, M. Mansouri, J. A. Nelson, and K. Früh, “BST2/tetherin enhances entry of human cytomegalovirus,” *PLoS Pathog.*, vol. 7, no. 11, 2011, doi: 10.1371/journal.ppat.1002332.

[57] S. Rangasamy, P. G. Mcguire, C. F. Nitta, F. Monickaraj, S. R. Oruganti, and A. Das, “Chemokine Mediated Monocyte Trafficking into the Retina : Role of Inflammation in Alteration of the Blood- Retinal Barrier in Diabetic Retinopathy,” vol. 9, no. 10, pp. 1–10, 2014, doi: 10.1371/journal.pone.0108508.

[58] G. Conductier, N. Blondeau, A. Guyon, J. L. Nahon, and C. Rovère, “The role of monocyte chemoattractant protein MCP1/CCL2 in neuroinflammatory diseases,” *J. Neuroimmunol.*, vol. 224, no. 1–2, pp. 93–100, 2010, doi: 10.1016/j.jneuroim.2010.05.010.

[59] M. Motwani, S. Pesiridis, and K. A. Fitzgerald, “DNA sensing by the cGAS–STING pathway in health and disease,” *Nat. Rev. Genet.*, vol. 20, no. 11, pp. 657–674, 2019, doi: 10.1038/s41576-019-0151-1.

[60] O. M. Koper, J. Kaminska, K. Sawicki, and H. Kemona, “CXCL9, CXCL10, CXCL11, and their receptor (CXCR3) in neuroinflammation and neurodegeneration,” *Adv. Clin. Exp. Med.*, vol. 27, no. 6, pp. 849–856, 2018, doi: 10.17219/acem/68846.

[61] D. Ron *et al.*, “Fibroblast growth factor receptor 4 is a high affinity receptor for both acidic and basic fibroblast growth factor but not for keratinocyte growth factor,” *J. Biol. Chem.*, vol. 268, no. 8, pp. 5388–5394, 1993, doi: 10.1016/s0021-9258(18)53334-2.

[62] A. Zani and J. S. Yount, “Antiviral Protection by IFITM3 In Vivo,” *Curr. Clin. Microbiol. Reports*, vol. 5, no. 4, pp. 229–237, 2018, doi: 10.1007/s40588-018-0103-0.

[63] F. McNab, K. Mayer-Barber, A. Sher, A. Wack, and A. O’Garra, “Type I interferons in infectious disease,” *Nat. Rev. Immunol.*, vol. 15, no. 2, pp. 87–103, 2015, doi: 10.1038/nri3787.

[64] C. Dinarello, “Biologic basis for interleukin-1 in disease,” *Blood*, vol. 87, no. 6, pp. 2095–2147, Mar. 1996, doi: 10.1182/blood.V87.6.2095.bloodjournal8762095.

[65] R. K. Kutty *et al.*, “Proinflammatory cytokines decrease the expression of genes critical for RPE function.,” *Mol. Vis.*, vol. 22, no. October, pp. 1156–1168, 2016.

[66] T. Tanaka, M. Narazaki, and T. Kishimoto, “IL-6 in Inflammation, Immunity, and Disease,” vol. 6, no. Kishimoto 1989, pp. 1–16, 2014.

[67] J. Sharma, S. Bhar, and C. S. Devi, “A review on interleukins: The key manipulators in rheumatoid arthritis,” *Mod. Rheumatol.*, vol. 27, no. 5, pp. 723–746, 2017, doi: 10.1080/14397595.2016.1266071.

[68] M. Buxadé *et al.*, “Gene expression induced by Toll-like receptors in macrophages requires the transcription factor NFAT5,” *J. Exp. Med.*, vol. 209, no. 2, pp. 379–393, 2012, doi: 10.1084/jem.20111569.

[69] Q. Li and I. M. Verma, “NF-κB regulation in the immune system,” *Nat. Rev. Immunol.*, vol. 2, no. 10, pp. 725–734, 2002, doi: 10.1038/nri910.

[70] K. J. Helbig and M. R. Beard, “The role of viperin in the innate antiviral response,” *J. Mol. Biol.*, vol. 426, no. 6, pp. 1210–1219, 2014, doi: 10.1016/j.jmb.2013.10.019.

[71] M. Hösel *et al.*, “Toll-like receptor 2-mediated innate immune response in human nonparenchymal liver cells toward adeno-associated viral vectors,” *Hepatology*, vol. 55, no. 1, pp. 287–297, 2012, doi: 10.1002/hep.24625.

[72] A. Klettner, T. Hamann, K. Schlüter, R. Lucius, and J. Roider, “Retinal pigment epithelium cells alter the pro-inflammatory response of retinal microglia to TLR-3 stimulation,” *Acta Ophthalmol.*, vol. 92, no. 8, pp. e621–e629, 2014, doi: 10.1111/aos.12472.

[73] C. Zannetti *et al.*, “TLR9 Transcriptional Regulation in Response to Double-Stranded DNA Viruses,” *J. Immunol.*, vol. 193, no. 7, pp. 3398–3408, 2014, doi: 10.4049/jimmunol.1400249.

[74] A. M. Krieg, “Antiinfective applications of toll-like receptor 9 agonists,” *Proc. Am. Thorac. Soc.*, vol. 4, no. 3, pp. 289–294, 2007, doi: 10.1513/pats.200701-021AW.

[75] W. Xiong *et al.*, “ AAV cis -regulatory sequences are correlated with ocular toxicity ,” *Proc. Natl. Acad. Sci.*, vol. 116, no. 12, pp. 5785–5794, 2019, doi: 10.1073/pnas.1821000116.

[76] L. Zhang *et al.*, “Genetic Rescue Reverses Microglial Activation in Preclinical Models of Retinitis Pigmentosa,” *Mol. Ther.*, vol. 26, no. 8, pp. 1953–1964, 2018, doi: 10.1016/j.ymthe.2018.06.014.

[77] C. Vijayasarathy, Y. Zeng, M. J. Brooks, R. N. Fariss, and P. A. Sieving, “ Genetic

Rescue of X-Linked Retinoschisis Mouse (Rs1 −/y) Retina Induces Quiescence of the Retinal Microglial Inflammatory State Following AAV8- RS1 Gene Transfer and Identifies Gene Networks Underlying Retinal Recovery ," *Hum. Gene Ther.*, vol. 00, no. 00, pp. 1–15, 2020, doi: 10.1089/hum.2020.213.

[78] W. Yu *et al.*, "Nrl knockdown by AAV-delivered CRISPR/Cas9 prevents retinal degeneration in mice," *Nat. Commun.*, vol. 8, pp. 1–15, 2017, doi: 10.1038/ncomms14716.

[79] L. Toualbi, M. Toms, and M. Moosajee, "The landscape of non-viral gene augmentation strategies for inherited retinal diseases," *Int. J. Mol. Sci.*, vol. 22, no. 5, pp. 1–14, 2021, doi: 10.3390/ijms22052318.

[80] K. W. Tsai *et al.*, "Difference in the regulation of IL-8 expression induced by uropathogenic E. coli between two kinds of urinary tract epithelial cells," *J. Biomed. Sci.*, vol. 16, no. 1, 2009, doi: 10.1186/1423-0127-16-91.